Copy 282

NACA RM A54K09

NACA

RESEARCH MEMORANDUM

LONGITUDINAL STABILITY CHARACTERISTICS AT MACH NUMBERS UP TO 0.92 OF A WING-BODY-TAIL COMBINATION HAVING A WING WITH 45° OF SWEEPBACK AND A TAIL IN VARIOUS VERTICAL POSITIONS

By Jack D. Stephenson, Angelo Bandettini, and Ralph Selan

Ames Aeronautical Laboratory
Moffett Field, Calif.

NATIONAL ADVISORY COMMITTEE FOR AERONAUTICS

WASHINGTON

January 28, 1955

NATIONAL ADVISORY COMMITTEE FOR AERONAUTICS

RESEARCH MEMORANDUM

LONGITUDINAL STABILITY CHARACTERISTICS AT MACH NUMBERS UP TO 0.92 OF A WING-BODY-TAIL COMBINATION HAVING A WING WITH 45° OF SWEEPBACK AND A TAIL IN VARIOUS VERTICAL POSITIONS

By Jack D. Stephenson, Angelo Bandettini, and Ralph Selan

SUMMARY

Wind-tunnel tests were conducted at Mach numbers from 0.25 to 0.92 to measure the static longitudinal stability characteristics of a semispan wing-fuselage-tail model having a wing with 45° of sweepback. The wing had an aspect ratio of 5.5 and had NACA 64A010 sections normal to the quarter-chord line. A plane, unswept, horizontal tail of aspect ratio 4 was mounted in four different vertical positions varying from 12.7-percent semispan below the wing chord plane extended to 25.5-percent semispan above the chord plane extended.

The center of pressure of the wing-fuselage combination moved forward as the wing began to stall, and a tail in the higher positions produced additional stalling moments due to high effective downwash. The loss of tail contribution due to the downwash was delayed to higher angles of attack when the tail was lowered to the wing chord plane extended.

The addition of leading-edge fences or of leading-edge chord extensions reduced the forward center-of-pressure movement of the wing-fuselage combination and the losses in tail contribution that occurred when the wing stalled.

INTRODUCTION

Existing results of aerodynamic studies of wings similar in plan form to the one employed on the model which is the subject of this report indicate that the combination of plan form and section selected for this model would have high aerodynamic efficiency at high subsonic Mach numbers (refs. 1 and 2). The tests reported herein were undertaken to obtain further information applicable to a complete airplane configuration suitable for superior long-range performance at high subsonic speeds. Previous tests of wings of this general plan form indicate that at high lift coefficients they are subject to severe longitudinal instability as a result of an extreme forward movement of the center of pressure which results from separation of the flow at the wing tips.

Tests such as those reported in references 3 and 4 of wing-body-tail combinations have shown that the contribution of the tail to the stability is of a regular nature and can generally be predicted when the wing is unstalled. However, when separation occurs on the wing, it has been observed that high downwash may occur at certain possible tail locations, causing more severe longitudinal instability than that due to the wing and fuselage. Other tail locations have been observed where the reductions in stability of the wing-fuselage combinations are partially or completely compensated for by simultaneous increases in the contribution of the tail to stability (see refs. 5 and 6).

Reference 2, which presents data from tests of a model having the wing used in the tests described in the present report and having a similar fuselage, indicates that the model was not subject to large adverse effects of compressibility on minimum drag or on maximum lift-drag ratio up to high subsonic Mach numbers. The tests reported herein were intended to ascertain to what degree the severe static longitudinal instability of the wing-fuselage combination might be avoided in the case of a model with a horizontal tail. The means of avoiding or reducing this instability included varying the vertical position of the horizontal tail and adding fences and chord extensions to the wing.

A continuing part of this program is aimed at obtaining more detailed information indicating local flow characteristics in the region of the tail of this model, which it is hoped will afford a basis for improved methods of estimating downwash behind swept wings.

NOTATION

a_t	lift-curve slope of the isolated tail
a_{w+b}	lift-curve slope of the wing-fuselage combination
a_{w+b+t}	lift-curve slope of the wing-fuselage-tail combination
b	wing span
c	local wing chord parallel to the plane of symmetry
$\bar{c}$	wing mean aerodynamic chord, $\dfrac{\int_0^{b/2} c^2 dy}{\int_0^{b/2} c\, dy}$
C_D	drag coefficient, $\dfrac{\text{drag}}{qS_w}$
C_L	lift coefficient, $\dfrac{\text{lift}}{qS_w}$

C_m pitching-moment coefficient about the quarter-chord point of the wing mean aerodynamic chord, $\frac{\text{pitching moment}}{qS_w\bar{c}}$

i_t incidence of the horizontal tail measured from the body center line, deg

l length of the body

l_t tail length, distance from the quarter-chord point of the wing mean aerodynamic chord to the quarter-chord point of the horizontal-tail mean aerodynamic chord

M free-stream Mach number

q free-stream dynamic pressure

q_t effective dynamic pressure at the tail

R Reynolds number based on wing mean aerodynamic chord

r local radius of body

r_o maximum radius of body

S_w area of basic semispan wing

S_t area of semispan tail

V_t horizontal-tail volume, $\frac{S_t l_t}{S_w \bar{c}}$

x longitudinal distance

y lateral distance from plane of symmetry

α angle of attack, deg

α_t tail angle of attack, deg

ϵ downwash angle, deg

η tail efficiency

MODEL AND APPARATUS

Figure 1 is a sketch of the model. The model consisted of a semispan wing, fuselage, and horizontal tail. The wing was constructed of solid aluminum alloy and had 45° of sweepback at the quarter-chord line, an aspect ratio of 5.50, a taper ratio of 0.53 and was without twist. The airfoil section normal to the quarter-chord line was the NACA 64A010.

The fuselage, a half-body of revolution of fineness ratio 12.5, was of cast aluminum mounted on a steel spar. The center line of the fuselage coincided with the wing-root chord line, and the quarter-chord position of the wing mean aerodynamic chord was alined with the midpoint of the body length.

The horizontal tail surface was mounted in positions representative of possible locations of the tail on a long-range airplane. The tail volume is also believed to have been typical of such an airplane. The geometry of the tail surface was selected because its aerodynamic characteristics indicated that it would be favorable for measuring effective downwash at the tail location. A similar surface was shown in reference 7 to be free from large or erratic compressibility effects throughout the Mach number range of the model tests and to have a lift curve that was linear within a wide angle-of-attack range. The tail surface represented an all-movable stabilizer having zero sweep of the midchord line, an aspect ratio of 4.0, a taper ratio of 0.5, and NACA 63A004 sections. The tail area was 24.8 percent of the wing area and the quarter-chord point of the tail mean aerodynamic chord was $2.0\bar{c}$ behind the quarter-chord point of the wing mean aerodynamic chord. Provision was made to mount the horizontal tail at four vertical positions, as follows: (a) a low position 12.7 percent of the wing semispan below the wing chord plane extended; (b) a center position in the wing chord plane extended; (c) a medium high position 12.7-percent semispan above the wing chord plane extended; and (d) a high position 25.5-percent semispan above the wing chord plane extended. The tail surface was supported in the three positions away from the fuselage center line by means of steel pylons. The junctures between the stabilizer and pylon were covered with a wood fairing as shown in figure 2(a). When the tail was mounted below the fuselage, an additional fairing was installed over the pylon surface between the juncture fairing and the fuselage (fig. 2(b)) in an effort to reduce interference at high angles of attack.

The fences shown in figure 1(b) were mounted on the wing during portions of the test at one or more of the following spanwise stations: $0.44b/2$, $0.57b/2$, $0.69b/2$, and $0.82b/2$. Figure 2(c) is a photograph of one combination of the fences. Provision was made for testing the fences with the rearward 50 percent or 75 percent removed. Leading-edge chord extensions were also installed on the outer portion of the wing during part of the test. These extensions (shown in figs. 1(b) and 2(d)) increased the local chord normal to the quarter-chord line by 15 percent and increased the streamwise chord by 17 percent. The inner ends of the chord extensions, which were located as indicated in figure 1(b), were plane surfaces parallel to the model plane of symmetry. The chord-extension section was similar to the forward part of the original section, except for a reduced thickness ratio and nose radius, and was faired into the basic wing section at its maximum thickness. Coordinates of the chord extensions in sections normal to the quarter-chord line of the original wing are given in table I. The wing area of the model was increased by 8 percent when the largest chord extension was installed.

Additional geometric data are listed in table II for the various model components.

TESTS

Experimental studies were conducted to determine the static longitudinal stability characteristics of the model without the tail and with the tail mounted at each of the four positions indicated in figure 1. With the tail at the fuselage center line and 12.7-percent semispan above the center line, its incidence was varied from 0° to -5°.

Effects of various fence installations upon the characteristics of the wing-fuselage combination were measured in a limited series of tests and one fence configuration was selected for more detailed stability studies. The effects of leading-edge chord extensions upon the longitudinal stability of the model were also investigated.

Measurements were made of lift, drag, and pitching moments at Mach numbers from 0.25 to 0.92 at a Reynolds number of 2,000,000. At a Mach number of 0.25, data were also obtained at a Reynolds number of 10,000,000.

CORRECTIONS TO DATA

The data have been corrected for constriction effects due to the presence of the tunnel walls, for tunnel-wall interference effects originating from lift on the model, and for the drag tares caused by aerodynamic forces on the exposed portion of the turntable on which the model was mounted.

The dynamic pressure and the Mach number were corrected for constriction effects due to the presence of the tunnel walls by the methods of reference 8. The corrected and uncorrected Mach numbers and the ratio of corrected to uncorrected dynamic pressure are presented in table III(a). The correction to the drag coefficient for the effect of the pressure gradient due to the wake was estimated and found to be negligible.

Corrections for the effects of tunnel-wall interference due to model lift were calculated by the method of reference 9. The corrections (which were added to the data) were as follows:

$\Delta\alpha = K_1 C_L$	$\Delta C_m = K_2 C_L$	Model without tail
$\Delta C_D = 0.0053\ C_L^2$	$\Delta C_m = K_3 C_L$	Model with tail

The values of K_1, K_2, and K_3 are shown in table III(b) as functions of Mach number.

Since the turntable upon which the model was mounted was directly connected to the balance system, a tare correction to the drag was necessary. The magnitude of this correction was calculated by multiplying the forces on the turntable with the model removed by the fraction of the area of the turntable still exposed to the air stream after installation of the model. The tare corrections, converted to tare drag coefficients based on wing area, were substracted from the measured drag coefficients and are presented in table III(c). No attempt has been made to evaluate tares due to interference between the model and the turntable or to compensate for the tunnel-floor boundary layer, which at the turntable had a displacement thickness of one-half inch.

RESULTS AND DISCUSSION

Basic Model

The lift, drag, and moment characteristics of the wing-fuselage combination are presented in figures 3 and 4. These data are practically identical to those measured on a similar wing-body combination and reported in reference 2. Throughout the test range of Reynolds numbers and Mach numbers and at lift coefficients greater than about 0.6, the center of pressure of the wing-body combination moved forward rapidly with increasing angle of attack. As is well known, this behavior is a result of flow separation beginning at the wing tip and progressing inward with increasing angle of attack and is characteristic of wings of this general plan form. In addition to the data for the wing-fuselage combination, data are presented for the model with the three tail-mounting pylons and fairings, which, except for increasing slightly the level of the drag data, had only minor effects. Small differences in pitching moments for various tail-mounting pylons can be attributed to the fact that the characteristics at the stall were somewhat erratic and not repeatable.

Figures 5 and 6 show the effects of adding the horizontal-tail surface in various vertical positions. The pitching-moment data referred to the wing quarter-chord point indicate a considerable static margin for the angle-of-attack range where the lift curve remained linear. At the higher angles of attack, large and abrupt movements of the center of pressure occurred. These movements were greatest when the tail was in the highest position and decreased progressively as the tail was lowered. A detailed comparison of the pitching moments of the model with and without the tail (figs. 3 through 6) indicates that when the tail was 12.7-percent semispan below the fuselage, it contributed to the stability throughout the angle-of-attack range, whereas for higher tail locations, when wing stalling occurred, the tail contributed a powerful positive pitching moment.

The decreased static longitudinal stability near zero lift for the model with the tail at the fuselage center line is an indication of the effect of the wing wake. The data show that the pitching moment at zero lift varied with tail height, indicating a local flow at the tail directed inward toward the fuselage axis.

Effect of Fences

The effect of the location of full-chord fences was investigated at two Mach numbers by installing the fences in several combinations at one or more of the following stations: 0.44b/2, 0.57b/2, 0.69b/2, and 0.82b/2. The lift and moment characteristics of the model without the tail (fig. 7(a)) indicate that at a Mach number of 0.25 a single fence at 44-percent semispan increased the lift coefficients at which large forward center-of-pressure movements occurred and reduced the magnitude of these movements prior to the attainment of maximum lift. The least variation of center of pressure with lift coefficient resulted when two fences were used, one at 44-percent and one at 69-percent semispan. None of the fence combinations provided any substantial improvements at a Mach number of 0.9. It was expected that some insight into the origin of the improved stability due to the fences might be afforded if the chordwise extent of the fences were varied. Results of tests with two fences (at 44-percent and 69-percent semispan) having the after 75 percent and the after 50 percent of the fences removed are presented in figure 7(b). The data show that fences extending over only the forward 25 percent of the chord were almost as effective as any of the longer chord fences, indicating that the effects of separation on this wing were most strongly influenced by the flow near the leading edge. The full-chord fences resulted in slightly higher values for the lift coefficient at which the center of pressure moved forward. On the basis of these limited tests of the model without the tail, the full-chord fences at 0.44 and 0.69 semispan were selected to be tested in more detail.

The lift, drag, and moment characteristics of the model without the tail and with full-chord fences at 0.44 and 0.69 semispan are shown in figure 8 at Mach numbers from 0.25 to 0.92 and a Reynolds number of 2,000,000. At all these Mach numbers the fences reduced the forward center-of-pressure movement accompanying stalling of the wing (prior to maximum lift) and at Mach numbers up to 0.85 substantially increased the lift coefficient at which instability occurred. The addition of the fences had very slight effect on the minimum drag and reduced the drag at moderate and high lift coefficients. At a Mach number of 0.92 there was some drag penalty due to the addition of fences.

Figure 9 shows the longitudinal characteristics of the model with fences and the various tail pylons at a Reynolds number of 10,000,000 and a Mach number of 0.25. Similar data for the Mach number range 0.25 to 0.92

at a Reynolds number of 2,000,000 are presented in figure 10. Comparison with the same type of data for the model without fences (figs. 3 and 4) indicates that the inconsistencies in the pitching-moment characteristics at the stall were somewhat reduced by the addition of fences.

Data for the model with fences and with the tail in various vertical positions are presented in figures 11 and 12 for Reynolds numbers of 10,000,000 and 2,000,000, respectively. With the tail in the high position, longitudinal instability occurred at angles of attack where the wing was partially stalled (as indicated by decreased lift-curve slopes). Lowering the tail decreased the magnitude of the instability and increased the angle of attack where it first occurred. With the tail in the chord plane extended, there were relatively small variations with lift coefficient of the center-of-pressure location, and the pitching-moment curves were considerably more linear than those for the model without fences. The improved stability for the higher tail positions was partly due to the effect mentioned previously of the fences on the stability of the wing-body combination. A detailed examination of the pitching moments of the model with fences both with and without the tail (figs. 9 through 12) has indicated that the tail did not contribute the large positive pitching moments which were observed for the model without fences, when the wing was partially stalled. Although the model was generally stable at maximum lift (in those cases when it was attained), with the tail in the two lower positions there was an abrupt change in pitching moment at high angles of attack prior to maximum lift. This is believed to have been due to stalling of the tail. Such stalling probably does not represent a flight problem for an airplane with a center-of-gravity location that would normally be employed because of the decrease in tail incidence that would be necessary for longitudinal balance in flight at these lift coefficients.

Effects of Chord Extensions

The lift and moment data measured at a Mach number of 0.25 and a Reynolds number of 2,000,000 are presented in figure 13 for the wing-fuselage model with chord extensions of various spans. The greatest improvement in linearity of the pitching-moment data resulted when the leading-edge discontinuity was at the innermost location. The addition of a fence at this discontinuity produced no improvement. The effects of increased Mach number on the characteristics of the wing-fuselage combination with the two longest span chord extensions are shown in figure 14. The pitching-moment characteristics of the wing-fuselage model with chord extensions were similar to the characteristics of the model with fences. At Mach numbers up to 0.85, there were substantial increases in the lift coefficients where large center-of-pressure movements occurred, but at Mach numbers of 0.90 and 0.92, only slight increases in the lift coefficients are evident. Although the increased wing area due to adding the chord extensions increased the lift proportionately, this effect

accounts for less than a sixth of the measured increase in the lift coefficient at which longitudinal instability occurred at the lower speeds.

In order to determine whether the downwash at the tail would be significantly influenced by the span of the chord extension, tests were conducted with two of the more promising chord extensions, one extending from 44-percent semispan to the wing tip and the other from 57-percent semispan to the tip. As shown in figures 15 and 16, with the tail in the wing chord plane extended, large forward movements of the center of pressure were avoided almost up to the wing maximum lift when either of these chord extensions was employed. Raising the tail to the medium position (0.127b/2) had adverse effects upon the stability, particularly with the shorter span chord extension. The addition of the longer span chord extension resulted in stability characteristics of the complete model quite similar to those of the model with fences. Because there was no clear superiority in the characteristics of the model with chord extensions over those of the model with fences, this modification was not studied in more detail. The possibility exists that one wing leading-edge modification may have some advantage in drag over the other modifications, but it is believed that the tests reported herein are inconclusive in this respect because the method of attaching the fences (fig. 2(c)) is certainly not optimum from the drag standpoint and because the basic-wing drag may have varied when the surface conditions were not sufficiently well duplicated each time the chord extensions were installed or removed.

Effectiveness of the Tail as an All-Movable Control

Figures 17 and 18 present data showing the effects of varying the tail incidence on the model without fences or chord extensions. At a Reynolds number of 10,000,000 (and Mach number of 0.25) figure 17 shows that varying the tail incidence from 0° to -5° was effective in varying the pitching moment at all angles of attack below maximum lift. Throughout the Mach number range at a Reynolds number of 2,000,000 (fig. 18), the stabilizer provided effective control until the effects of wing stalling upon the stability became large.

With two full-chord fences on the model, the data presented in figures 19 and 20 indicate that the stabilizer was effective until the wing stalled, but the effectiveness at the stall was erratic in some instances. Abrupt forward movements of the center of pressure occurred near maximum lift at some Mach numbers, but the magnitude of such movements was small when the tail incidence was -5°.

Characteristics at Low Lift Coefficients

The slope of the lift and pitching-moment curves and the variation of pitching-moment coefficient with stabilizer angle derived from data in the preceding figures are shown in figure 21. This figure shows dC_m/dC_L of the model without the tail at a lift coefficient of 0.1. This lift coefficient was selected to indicate the slope of the moment curve at low angles of attack and still avoid a discontinuity in the slope that characterized the data near zero lift at the higher Mach numbers with the tail off. Adding the fences caused the rearward movement of the aerodynamic center of the wing-fuselage combination at low angles of attack to occur at a lower Mach number. Data showing dC_m/dC_L of the complete model indicate that raising the tail from the fuselage center line to the medium (0.127b/2) position increased the static stability at zero lift. Adding fences produced no consistent effect on the stability of the complete model at zero lift. The stabilizer effectiveness dC_m/di_t at zero angle of attack shown in figure 21 as a function of Mach number indicates that increasing Mach number produced generally higher effectiveness, particularly when the tail was in the medium high location.

Tail Contribution to Stability

The force and pitching-moment data for the model with the medium and center-line tail locations (figs. 17 through 20) have been used to estimate the effective downwash angles shown in figures 22 and 23 as functions of angle of attack. (In order to estimate the downwash at high angles of attack, it was necessary to assume that the stabilizer effectiveness data could be extrapolated to include negative angles of incidence of the tail that were beyond the range of the experimental data.)

In figure 22 and at the top of figure 23 the effective downwash data at a Mach number of 0.25 are shown at two Reynolds numbers, 10,000,000 and 2,000,000, respectively. At both Reynolds numbers, the slopes of the downwash curves for the model without fences increased sharply at angles of attack slightly exceeding those where wing-body instability occurred. At all of the Mach numbers of the test (at a Reynolds number of 2,000,000) the slope of the downwash curves increased with angle of attack, but, when the tail was lowered to the center line, this increase was delayed to higher angles of attack (see fig. 23). The effects of adding fences are also shown in figures 22 and 23. The most significant effect was to decrease the downwash at the higher angles of attack, particularly in the region of the medium tail.

Force and pitching-moment data for the model with and without the tail, and force data for the isolated tail have been used to calculate the contribution of the horizontal tail to the longitudinal stability, as expressed in the following formula.

$$\left(\frac{dC_m}{dC_L}\right)_t = -V_t \frac{a_t}{a_{w+b}} \left[\eta \frac{q_t}{q} \left(1 - \frac{d\epsilon}{d\alpha}\right) + \alpha_t \frac{\partial\left(\eta \frac{q_t}{q}\right)}{\partial\alpha} \right]$$

This expression for the tail stability parameter $(dC_m/dC_L)_t$, which is the variation of pitching-moment coefficient due to the tail with lift coefficient of the wing-fuselage combination, affords a useful indication of the way the separate factors affect the tail contribution to the pitching moment of the model. This parameter is related to the increment due to the tail in the stability of the complete model by the expression

$$\left(\frac{dC_{m_t}}{dC_L}\right)_{w+b+t} = \frac{a_{w+b}}{a_{w+b+t}} \left(\frac{dC_m}{dC_L}\right)_t$$

The terms in the expression for the tail stability parameter were evaluated as follows: The lift-curve slope of the isolated tail a_t estimated from references 7 and 10 was measured at the average effective tail angle of attack as indicated by the effective downwash data. It was assumed that the Mach number at the tail was the same as the free-stream Mach number. The lift-curve slope of the wing-fuselage combination a_{w+b} was measured from data presented in figures 3, 4, 9, and 10. The product of the tail efficiency and the dynamic pressure at the tail $\eta(q_t/q)$ was computed from the relation $\eta \frac{q_t}{q} = -\frac{dC_m/di_t}{V_t a_t}$ where dC_m/di_t is the stabilizer effectiveness measured at constant model angle of attack. In calculating the tail contribution, the term $\alpha_t \frac{\partial\left(\eta \frac{q_t}{q}\right)}{\partial\alpha}$ was neglected.

The variations of the tail contribution to the stability and the factors making up this contribution are shown in figure 24 for a Reynolds number of 10,000,000 and a Mach number of 0.25, and in figure 25 for a Reynolds number of 2,000,000 and Mach numbers of 0.6, 0.8, and 0.9. Although the factor a_t/a_{w+b} and the tail-efficiency and dynamic-pressure factors indicated sizable variations with angle of attack for all the conditions shown, they did not appear to be of major importance in determining the effect of the vertical location of the tail. A comparison of the variations with angle of attack of the downwash factor $(1 - d\epsilon/d\alpha)$

and the tail stability parameter $(dC_m/dC_L)_t$ indicates that practically all of the significant characteristics of the latter can be traced to variations in downwash. At Mach numbers at least up to 0.9, rapid increase of effective downwash at the tail with increasing angle of attack resulted in decreased contribution of the tail to stability. When the tail was lowered from the medium to the center position, this decrease was delayed to higher angles.

The effects of adding fences to the model were to reduce or eliminate large erratic variations of $(dC_m/dC_L)_t$ at high angles of attack and under some of the test conditions to eliminate a loss of tail contribution that occurred as the wing first began to stall. This loss in tail contribution for the model without fences is the most noticeable in the data for the medium tail height and was still present to a lesser degree when fences were installed. At each of the test conditions shown, when such a loss occurred, it was diminished or avoided by lowering the tail to the model center line.

The large variations that are apparent in the factor $(1 - d\epsilon/d\alpha)$ may give rise to speculation as to the accuracy of such data, in view of the difficulty in calculating effective downwash from data in which the pitching moments are erratic. Although large and abrupt changes in the pitching-moment coefficient were measured when stalling of the wing occurred, it is believed that by careful examination of the moment data it has been possible to determine effective downwash angles that are at least qualitatively reliable and do not include important effects of dispersion or other inaccuracies.

Figure 25 includes some values of $\eta(q_t/q)$ which appear to be too high, exceeding unity at Mach numbers of 0.6 and 0.8 at high angles of attack. These values were calculated at conditions where the tail was at high angles of attack and may be in error as a result of factors that could not be properly accounted for in the method of calculation used. The pitching-moment data indicate that the tail was more effective at high angles of attack than would be predicted from estimates based on the lift curve of the isolated tail. The differences appear to result from differences in the shape of the lift curves of the tail when it was on the model as compared to the isolated tail, and are probably associated with local characteristics of the flow in the vicinity of the tail, such as the spanwise distribution of the downwash and the turbulence level of the flow near the tail. It is believed that the data presented for these angles of attack still provide a valid indication, at least qualitatively, of variations in tail contribution to pitching moment and the factors that most affect it.

Tail Incidence for Balance

Figure 26 shows the tail incidence required for longitudinal balance as a function of lift coefficient for the model with the tail in the chord plane extended (center position) and in the medium high position. The center of gravity was in all cases assumed to be at 44 percent of the mean aerodynamic chord. This location was selected as the most rearward point at which a static margin of 5-percent mean aerodynamic chord could be maintained throughout the range of Mach numbers at low to moderate angles of attack and was governed by the stability characteristics of the model with the tail in the center location.

The severe instability of the model without fences and with the tail $0.127b/2$ above the wing chord plane is evidenced by the large positive incidence angles required for balance at lift coefficients near 0.9. These positive angles of incidence were estimated by extrapolating the data, since the tests included only negative and neutral settings of the tail. The data show that adding the fences had considerable effect in decreasing the magnitude of the instability and in reducing the range of C_L for which the instability occurred. When the tail was in the center position and with the center of gravity at $0.44\bar{c}$, the model with fences was stable at all the Mach numbers of the tests and at all lift coefficients, except just prior to the attainment of maximum lift. It would be expected that other tail locations above the center line but lower than the medium tail would also result in longitudinal stability under all these conditions.

In selecting the vertical location of the horizontal-tail surface on an airplane, considerations of ground clearance in the landing attitude, distance from the jet exhaust, and the vertical location and incidence of the wing relative to the fuselage often require that the tail be above the wing chord plane. Further tests would be desirable to determine the highest position where a tail might be mounted behind a wing similar to the one that is the subject of this report, so as to provide adequate stability throughout the range of speeds and altitudes that would be encountered in flight.

CONCLUSIONS

Wind-tunnel tests of a wing-fuselage-tail combination having a wing swept back 45° and an aspect ratio of 5.5 indicated the following conclusions.

1. A large and abrupt forward movement of the center of pressure of the wing-fuselage combination at high angles of attack was a source of static longitudinal instability of the complete model. When a tail was

added to the model in a position below the wing chord plane, the significant variations in stability at high angles of attack were still attributable to the wing-fuselage characteristics, but as the tail height was progressively increased to 0.255 semispan above the wing chord plane, the tail produced increasingly powerful positive pitching moments.

2. For the model both with and without the tail, leading-edge fences at 44-percent and 69-percent semispan reduced the forward center-of-pressure movement accompanying stalling of the wing (prior to maximum lift) and, at Mach numbers up to 0.85, substantially increased the lift coefficient at which instability occurred.

3. A leading-edge chord extension between the wing tip and the 44-percent semispan station resulted in an improvement in stability that was similar to that provided by the leading-edge fences.

4. At Mach numbers up to 0.9, rapid increase of effective downwash at the tail with increasing angle of attack resulted in decreased contribution of the tail to stability, but when the tail was lowered to the wing chord plane this decrease was delayed to higher angles of attack.

5. The effects of adding fences were to reduce or eliminate the decrease in the contribution of the tail to stability.

6. Significant variations of static longitudinal stability with lift coefficient are indicated in data for all the model configurations investigated, but the model with fences and with the tail near the wing chord plane would be stable at all of the Mach numbers of the test and at all lift coefficients (except those at or just prior to maximum lift) if the center of gravity were located so as to provide a minimum static margin at low angles of attack of 5 percent of the mean aerodynamic chord.

Ames Aeronautical Laboratory
National Advisory Committee for Aeronautics
Moffett Field, Calif., Nov. 9, 1954

REFERENCES

1. Johnson, Ben H., Jr., and Shibata, Harry H.: Characteristics Throughout the Subsonic Speed Range of a Plane Wing and of a Cambered and Twisted Wing, Both Having 45° of Sweepback. NACA RM A51D27, 1951.

2. Shibata, Harry H., Bandettini, Angelo, and Cleary, Joseph: An Investigation Throughout the Subsonic Speed Range of a Full-Span and a Semispan Model of a Plane Wing and a Cambered and Twisted Wing, all Having 45° of Sweepback. NACA RM A52D01, 1952.

3. Bandettini, Angelo, and Selan, Ralph: The Effects of Horizontal-Tail Height and a Partial-Span Leading-Edge Extension on the Static Longitudinal Stability of a Wing-Fuselage-Tail Combination Having a Sweptback Wing. NACA RM A53J07, 1954.

4. Tinling, Bruce E.: The Longitudinal Characteristics at Mach Numbers up to 0.9 of a Wing-Fuselage-Tail Combination Having a Wing With 40° of Sweepback and an Aspect Ratio of 10. NACA RM A52I19, 1952.

5. Foster, Gerald V., and Griner, Roland F.: Low-Speed Longitudinal and Wake Air-Flow Characteristics at a Reynolds Number of 5.5×10^6 of a Circular-Arc 52° Sweptback Wing With a Fuselage and a Horizontal Tail at Various Vertical Positions. NACA RM L51C30, 1951.

6. Salmi, Reino J., and Jacques, William A.: Effect of Vertical Location of a Horizontal Tail on the Static Longitudinal Stability Characteristics of a 45° Sweptback Wing Fuselage Combination of Aspect Ratio 8 at a Reynolds Number of 4.0×10^6. NACA RM L51J08, 1952.

7. Nelson, Warren H., Allen, Edwin C., and Krumm, Walter J.: The Transonic Characteristics of 36 Symmetrical Wings of Varying Taper, Aspect Ratio, and Thickness as Determined by the Transonic-Bump Technique. NACA RM A53I29, 1953.

8. Herriot, John G.: Blockage Corrections for Three-Dimensional-Flow Closed-Throat Wind Tunnels With Consideration of the Effect of Compressibility. NACA Rep. 995, 1950. (Formerly NACA RM A7B28).

9. Sivells, James C., and Salmi, Rachel M.: Jet-Boundary Corrections for Complete and Semispan Swept Wings in Closed Circular Wind Tunnels. NACA TN 2454, 1951.

10. Cahill, Jones F., and Gottlieb, Stanley M.: Low-Speed Aerodynamic Characteristics of a Series of Swept Wings Having NACA 65A006 Airfoil Sections. NACA RM L9J20, 1950.

TABLE I.- COORDINATES OF CHORD-EXTENSION SECTION NORMAL TO QUARTER-CHORD LINE

[All dimensions in percent of chord of original section]

Station	Ordinate
-15.0	0
-14.3	.80
-13.9	1.00
-13.0	1.30
-11.9	1.60
-10.0	2.00
-7.0	2.50
-3.0	3.00
2.2	3.50
8.5	4.00
17.0	4.50
25.3	4.80
35.1	4.97
40.0	5.00

TABLE II. - GEOMETRY OF THE MODEL

Wing (without leading-edge extension)	
Aspect ratio	5.50
Taper ratio	0.532
Sweep of quarter-chord line, deg	45
Section normal to quarter-chord line	NACA 64A010
Area (semispan), sq ft	3.812
Mean aerodynamic chord, ft	1.215
Dihedral	0
Incidence	0
Position on body	on axis
Wing leading-edge chord extension	
Streamwise distance to extended leading edge	0.17c
Locations of inboard ends of extensions	0.44b/2, 0.57b/2, 0.69b/2, 0.82b/2
Wing fences	
Distance ahead of wing leading edge	0.05c
Spanwise locations	0.44b/2, 0.57b/2, 0.69b/2, 0.82b/2
Chordwise extent (from leading edge)	0.25c, 0.50c, 1.00c
Fuselage	
Fineness ratio	12.5
Length, ft	7.292
Frontal area/wing area	0.035
Horizontal tail	
Aspect ratio	4.0
Taper ratio	0.5
Sweep, deg (50 percent chord)	0
Section	NACA 63A004
Area (semispan sq ft)	0.945
Tail length (l_t)	$2.0\bar{c}$
Vertical distance above wing chord plane extended	
Low tail	-0.127b/2
Center tail	0
Medium tail	0.127b/2
High tail	0.255b/2

TABLE III.- CORRECTIONS TO DATA

(a) Constriction due to tunnel walls

Corrected Mach number	Uncorrected Mach number	$\frac{q_{corrected}}{q_{uncorrected}}$
0.25	0.250	1.001
.6	.599	1.002
.8	.797	1.004
.85	.846	1.005
.9	.893	1.008
.92	.911	1.010

(b) Jet-boundary effects

M	$K_1 = \frac{\Delta\alpha}{C_L}$	$K_2 = \frac{\Delta C_m}{C_L}$ (wing body)	$K_3 = \frac{\Delta C_m}{C_L}$ (wing body tail)
0.25	0.349	-0.0011	0.0038
.6	.349	-.0010	.0052
.8	.349	-.0008	.0080
.85	.349	-.0006	.0095
.9	.349	-.0001	.0114
.92	.360	.0001	.0123

(c) Tare corrections

Reynolds number	Mach number	$C_{D_{tare}}$
10,000,000	0.25	0.0049
2,000,000	.25	.0050
2,000,000	.60	.0051
2,000,000	.80	.0057
2,000,000	.85	.0060
2,000,000	.90	.0064
2,000,000	.92	.0067

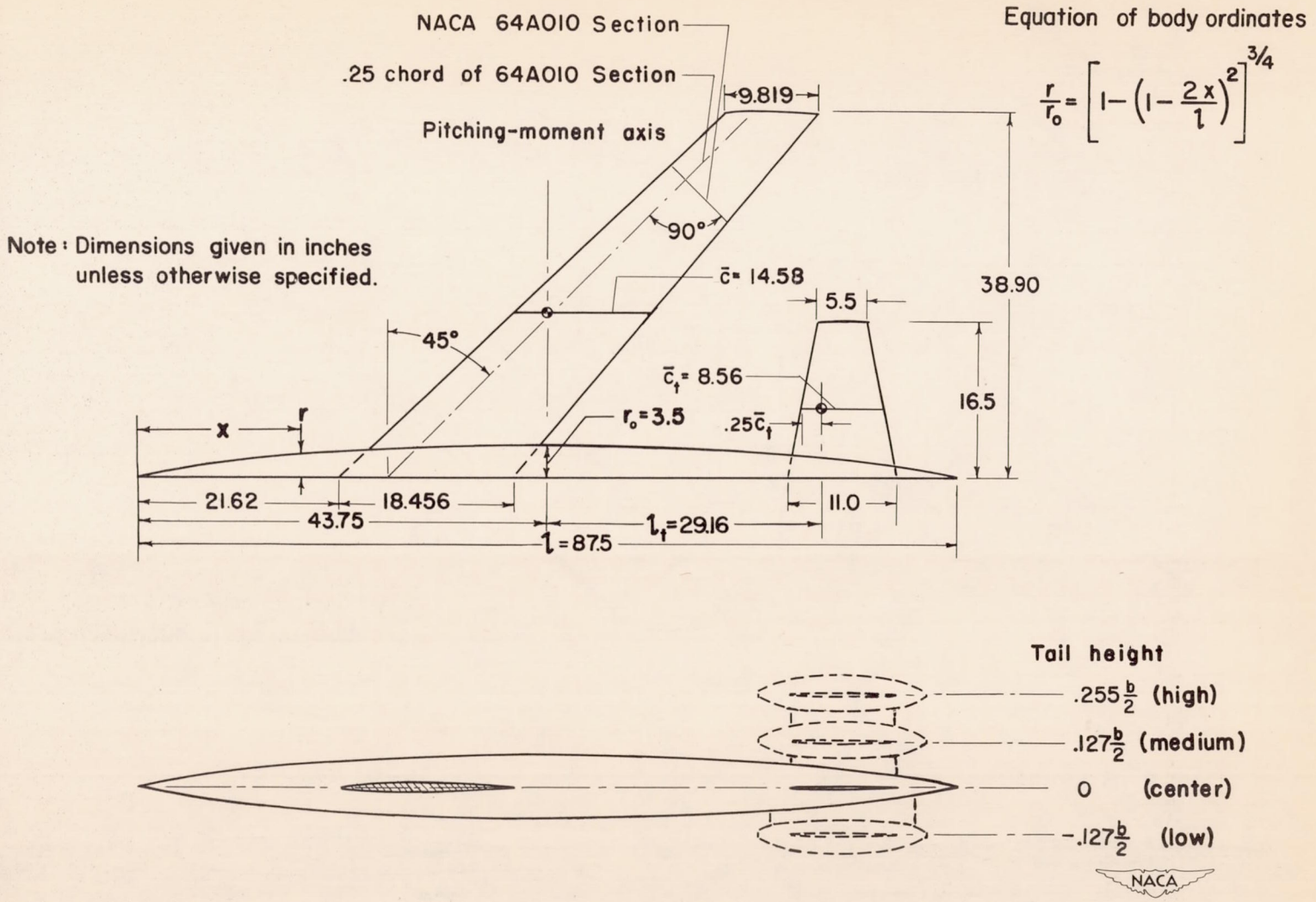

(a) Complete model and tail heights.

Figure 1.- Drawings of the model.

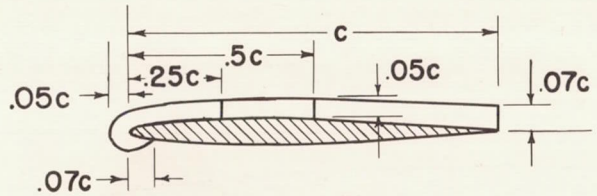

Section A-A

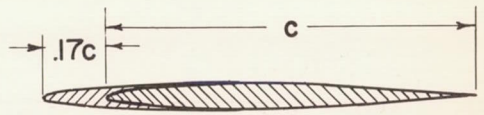

Section B-B

Note: Dimensions given in inches unless otherwise specified.

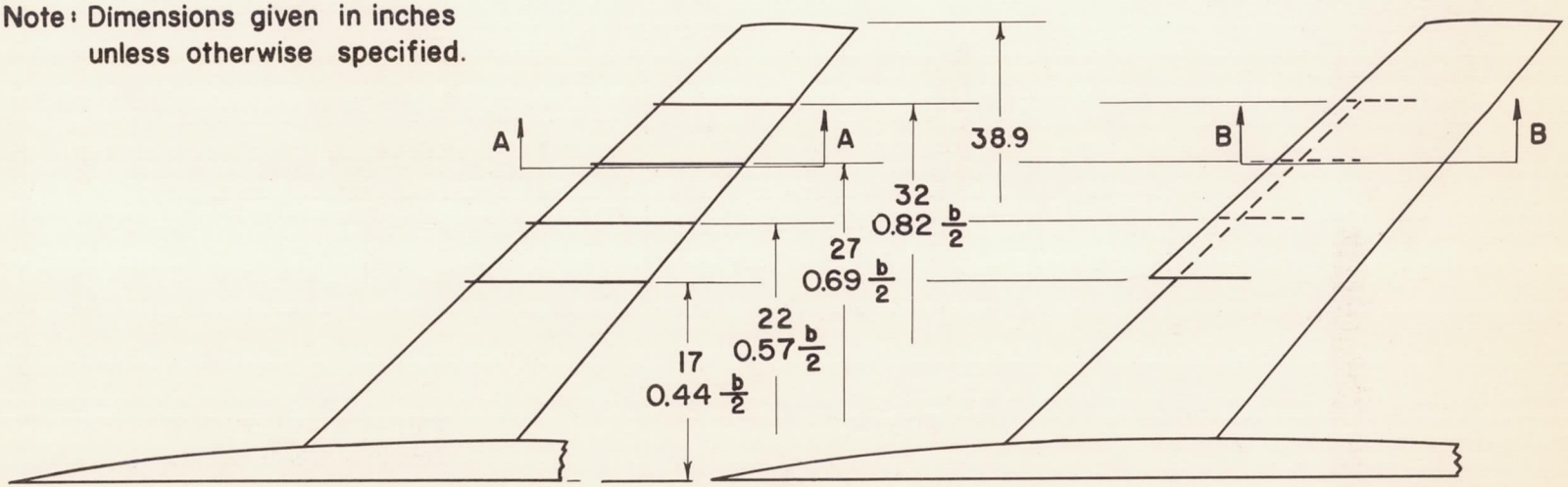

Fences

Chord extensions

NACA

(b) Fences and leading-edge extensions.

Figure 1.- Concluded.

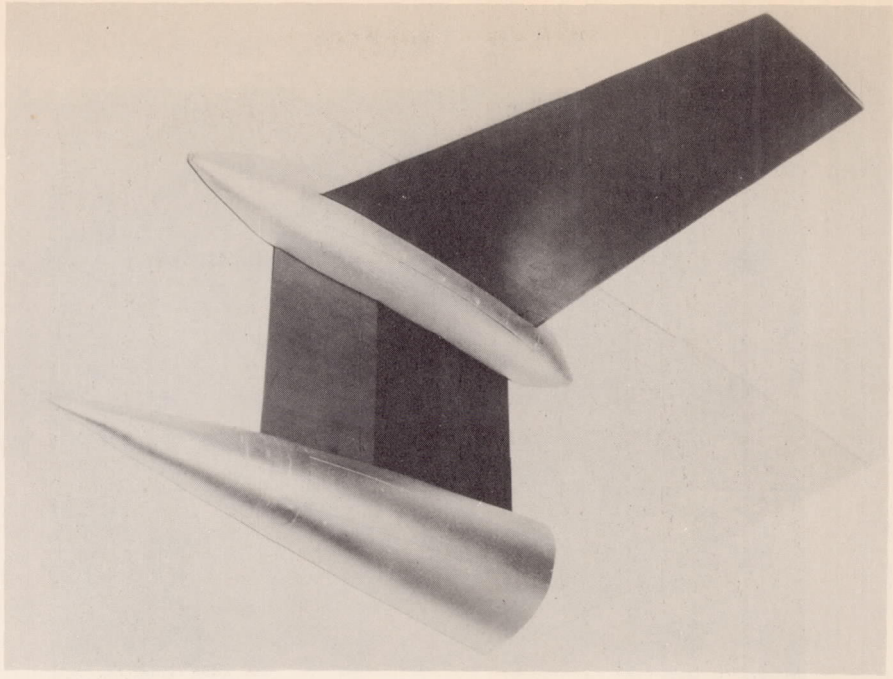

A-19237.1

(a) High tail position.

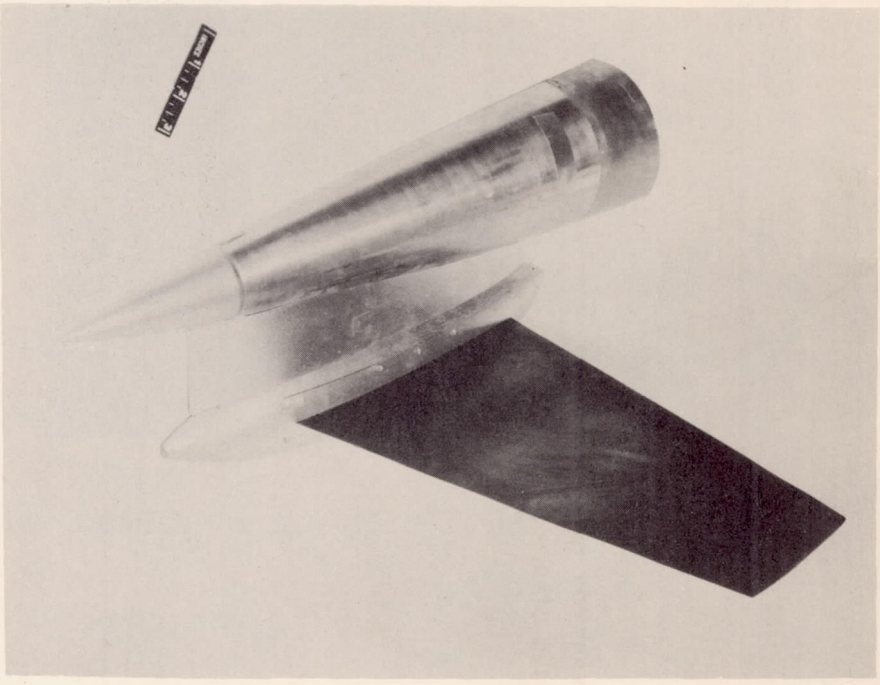

A-19238.1

(b) Low tail position.

Figure 2.- Photographs of the model.

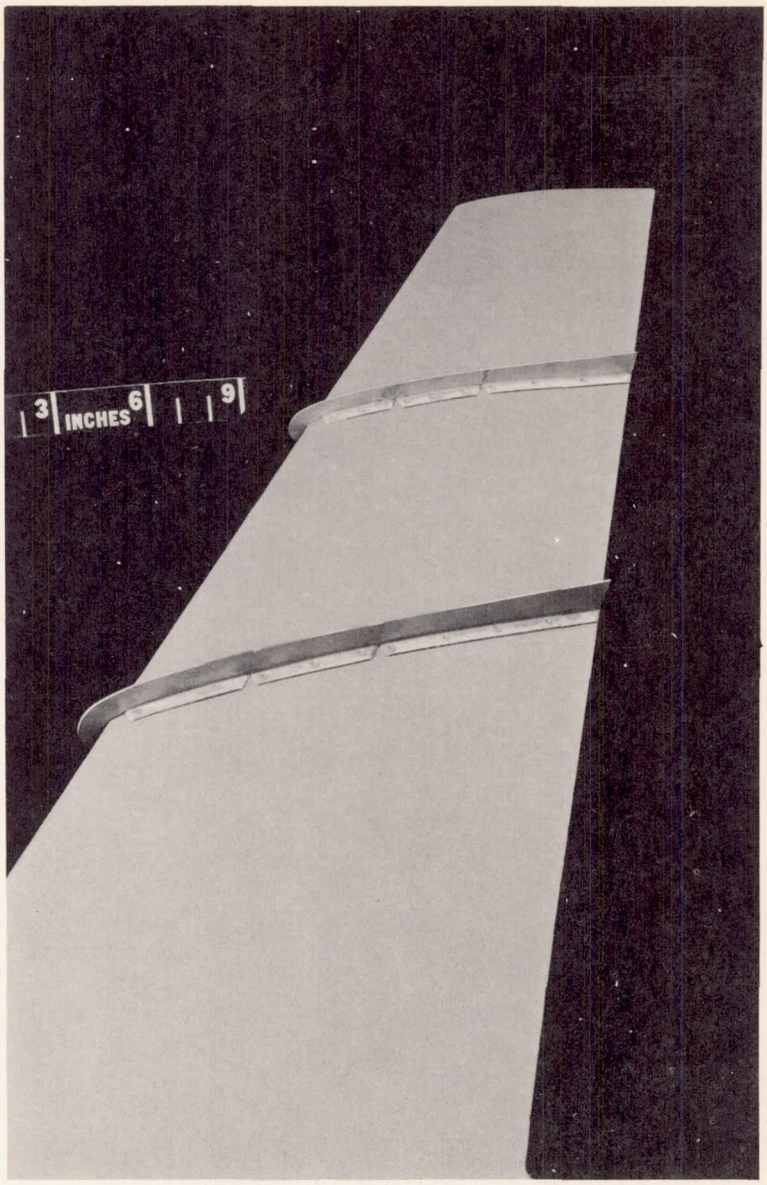

A-19782

(c) Full-chord fences at 0.44b/2 and 0.69b/2.

Figure 2.- Continued.

A-18987

(d) Model with a leading-edge chord extension between 0.44b/2 and the tip.

Figure 2.- Concluded.

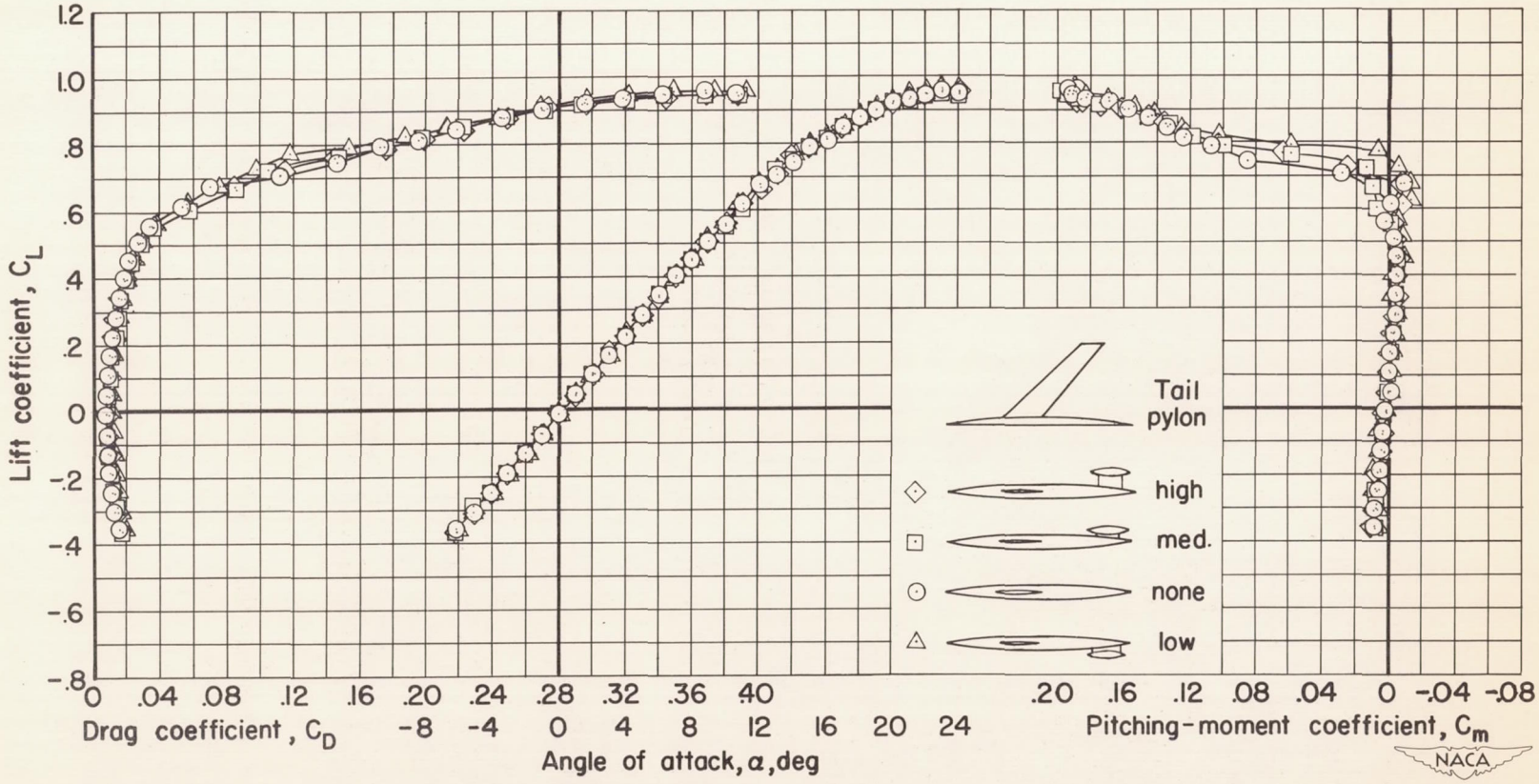

Figure 3.- The aerodynamic characteristics of the model with the tail off and with various tail support pylons at a Reynolds number of 10,000,000; M = 0.25.

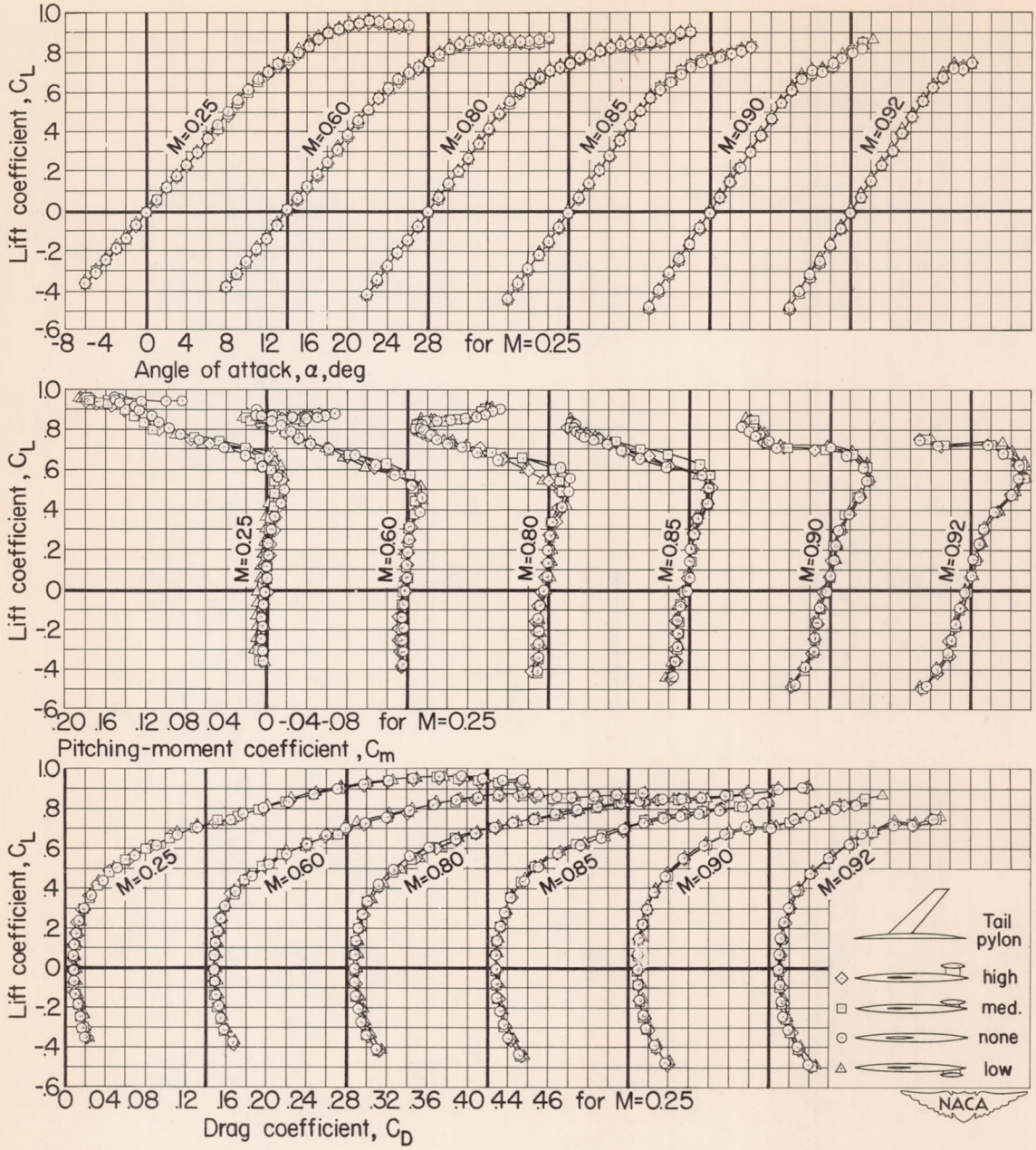

Figure 4.- The aerodynamic characteristics of the model with the tail off and with various tail support pylons at several Mach numbers; R = 2,000,000.

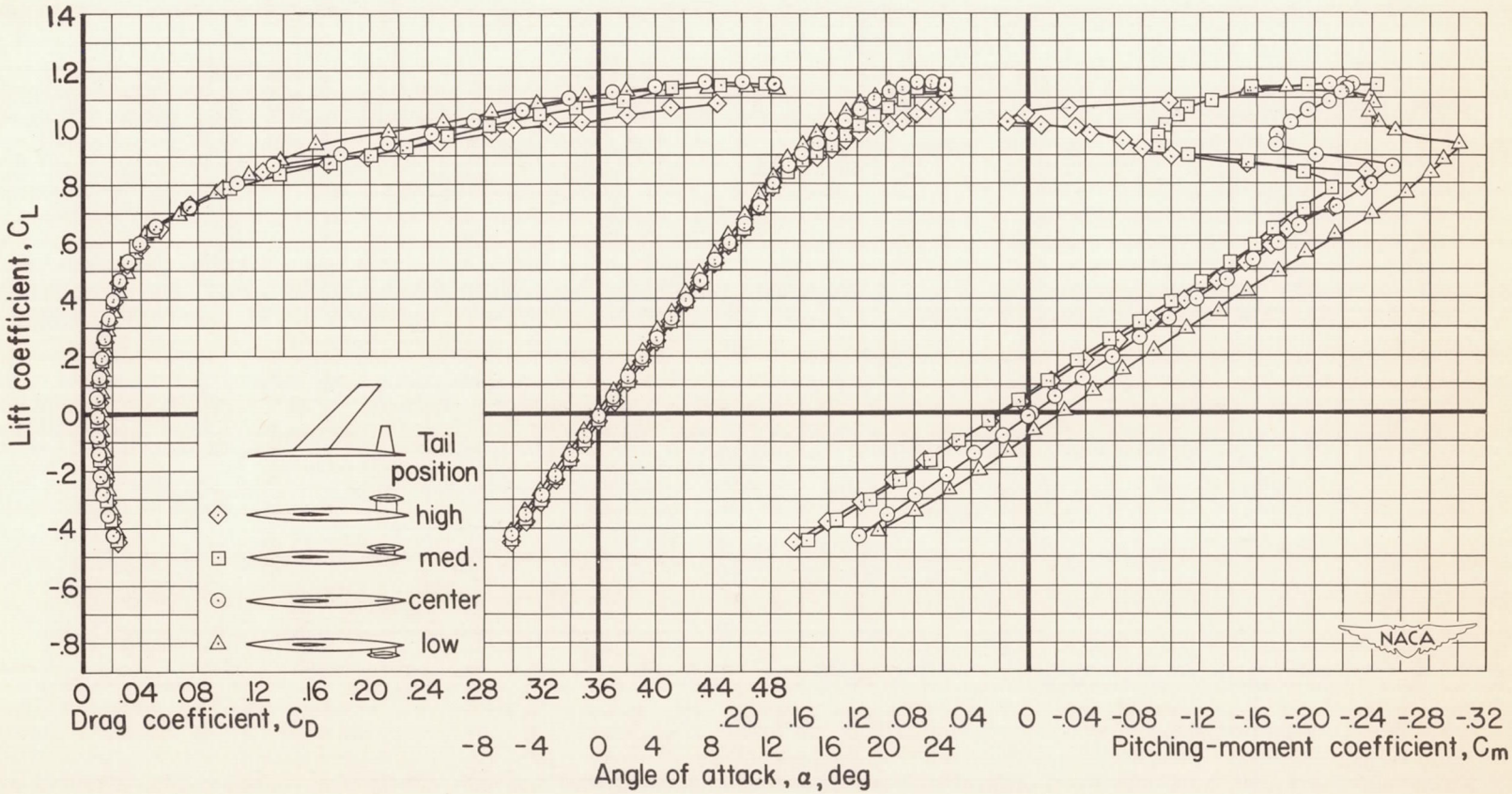

Figure 5.- The effect of tail height on the aerodynamic characteristics of the model at a Reynolds number of 10,000,000; M = 0.25.

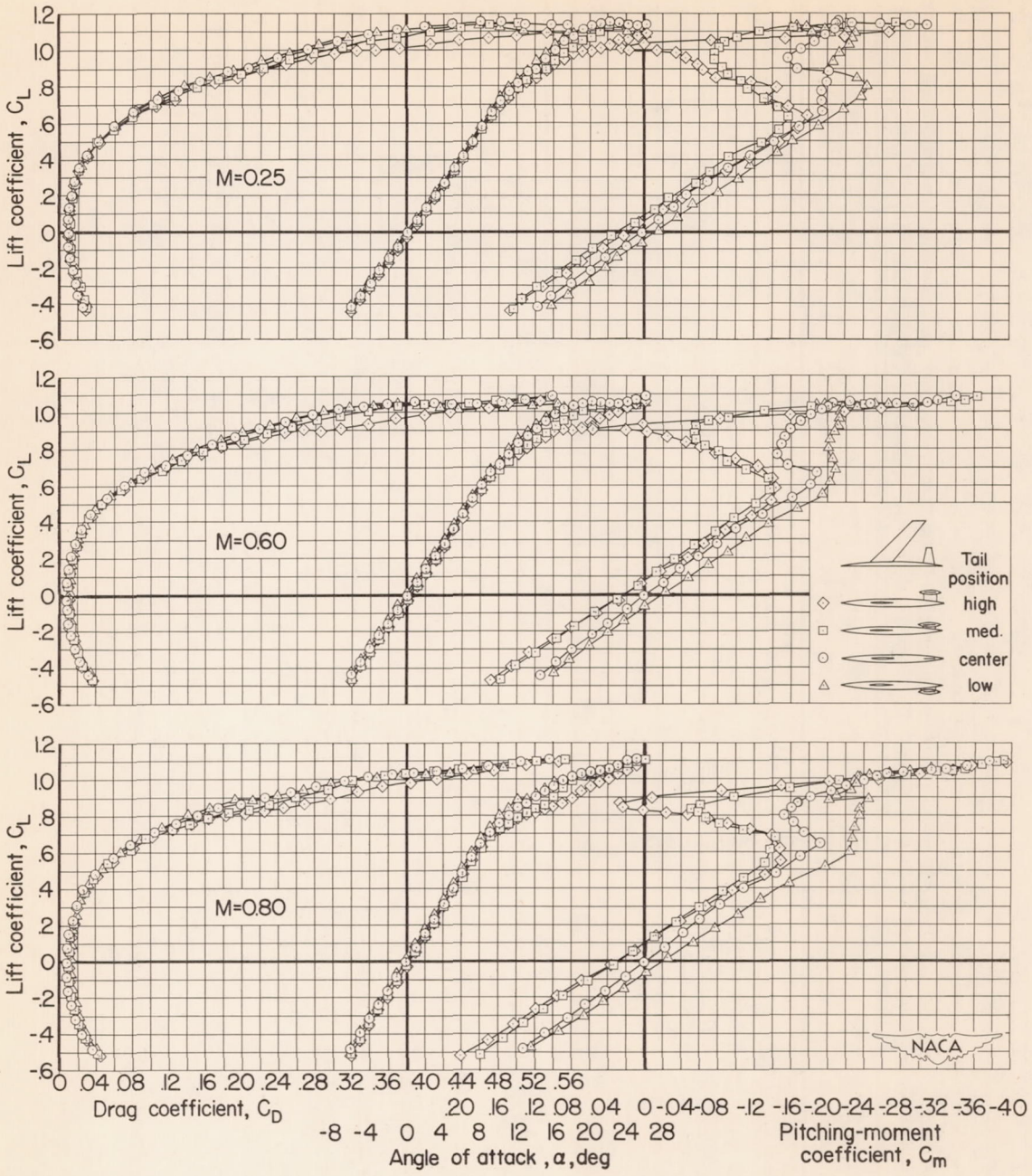

(a) M = 0.25, 0.60, and 0.80.

Figure 6.- The effect of tail height on the aerodynamic characteristics of the model at various Mach numbers; R = 2,000,000.

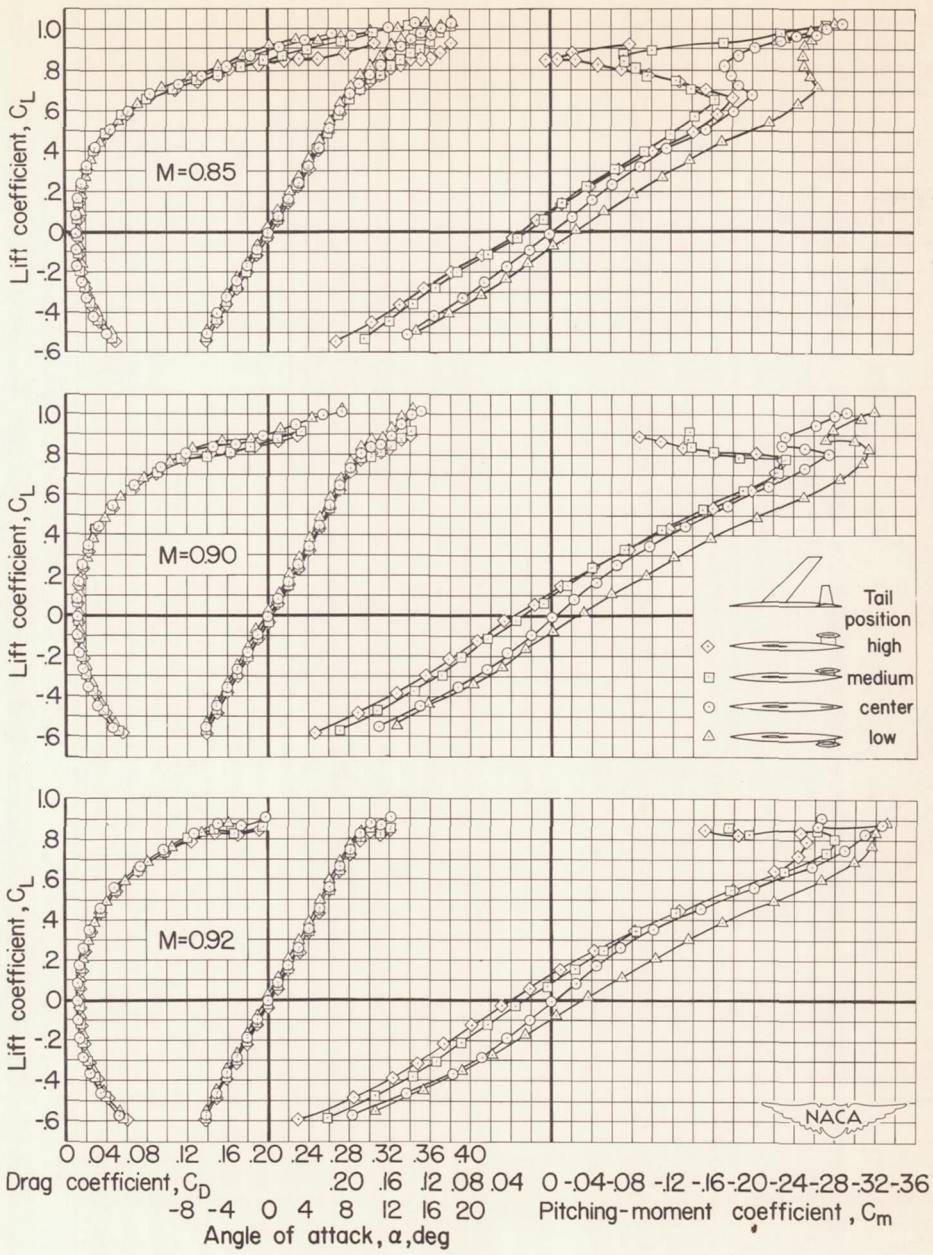

(b) M = 0.85, 0.90, and 0.92.

Figure 6.- Concluded.

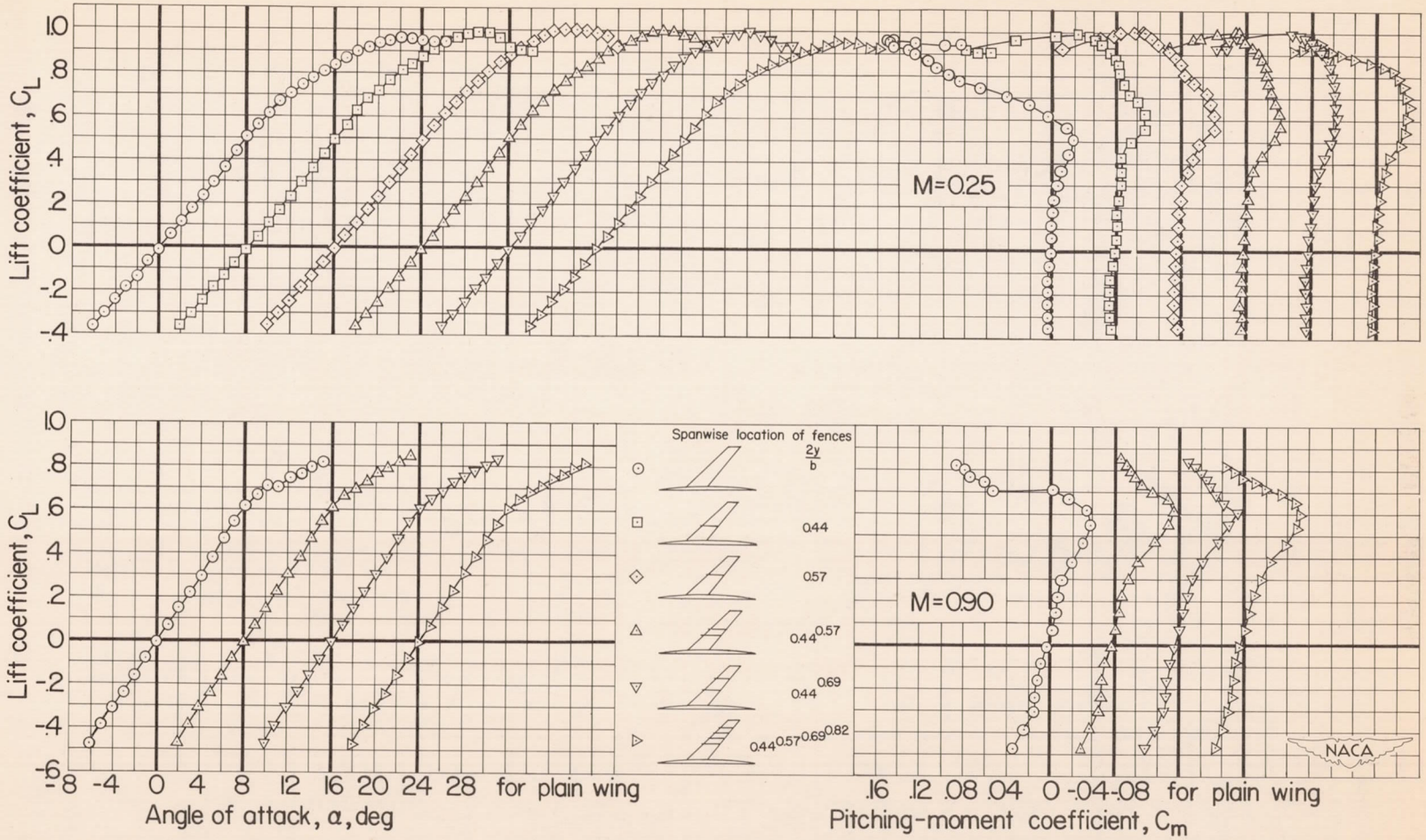

(a) Effect of span location.

Figure 7.- Lift and pitching-moment characteristics of the model with the tail off and with various combinations of fences at Mach numbers of 0.25 and 0.90; R = 2,000,000.

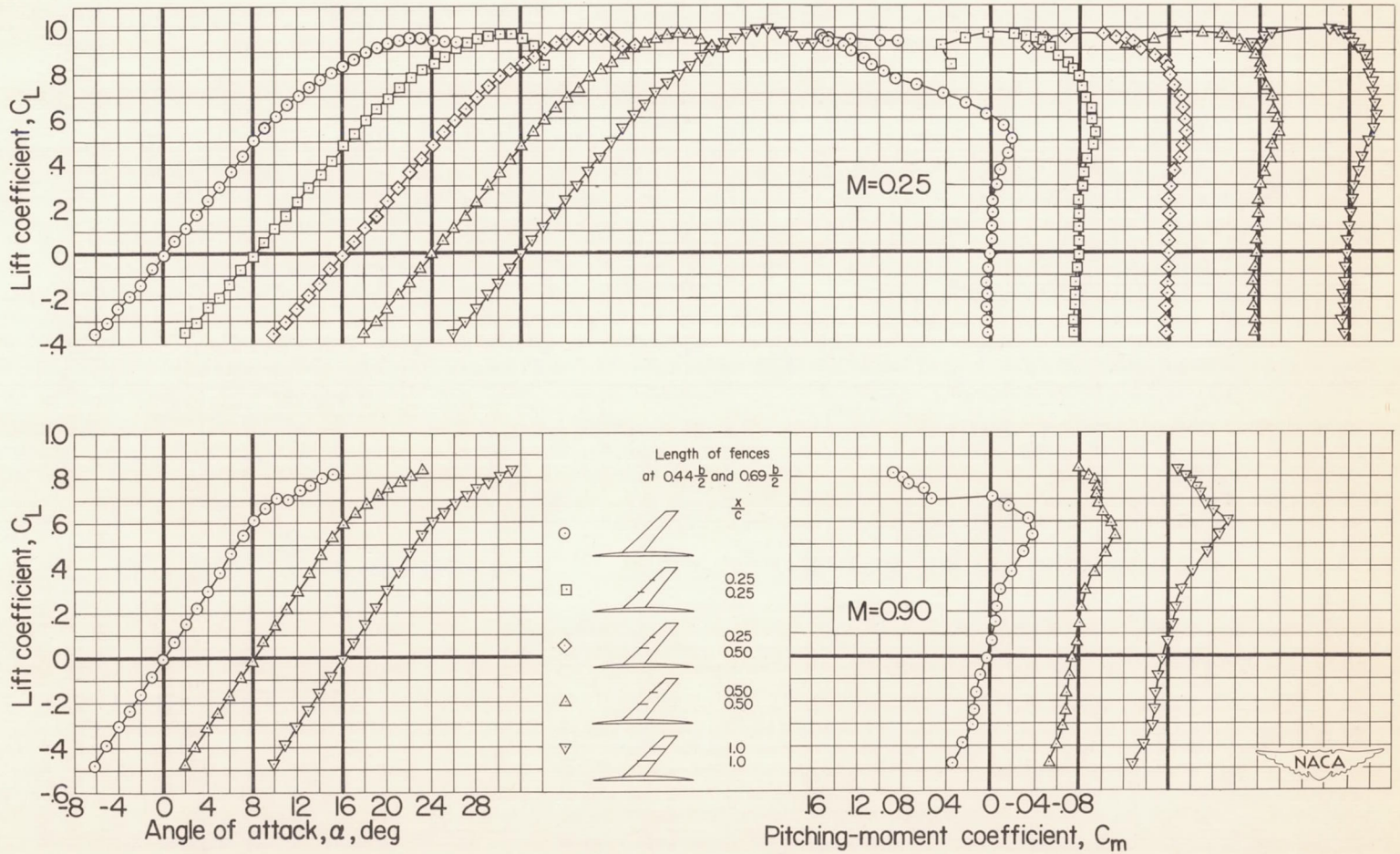

(b) Effect of fence length.

Figure 7.- Concluded.

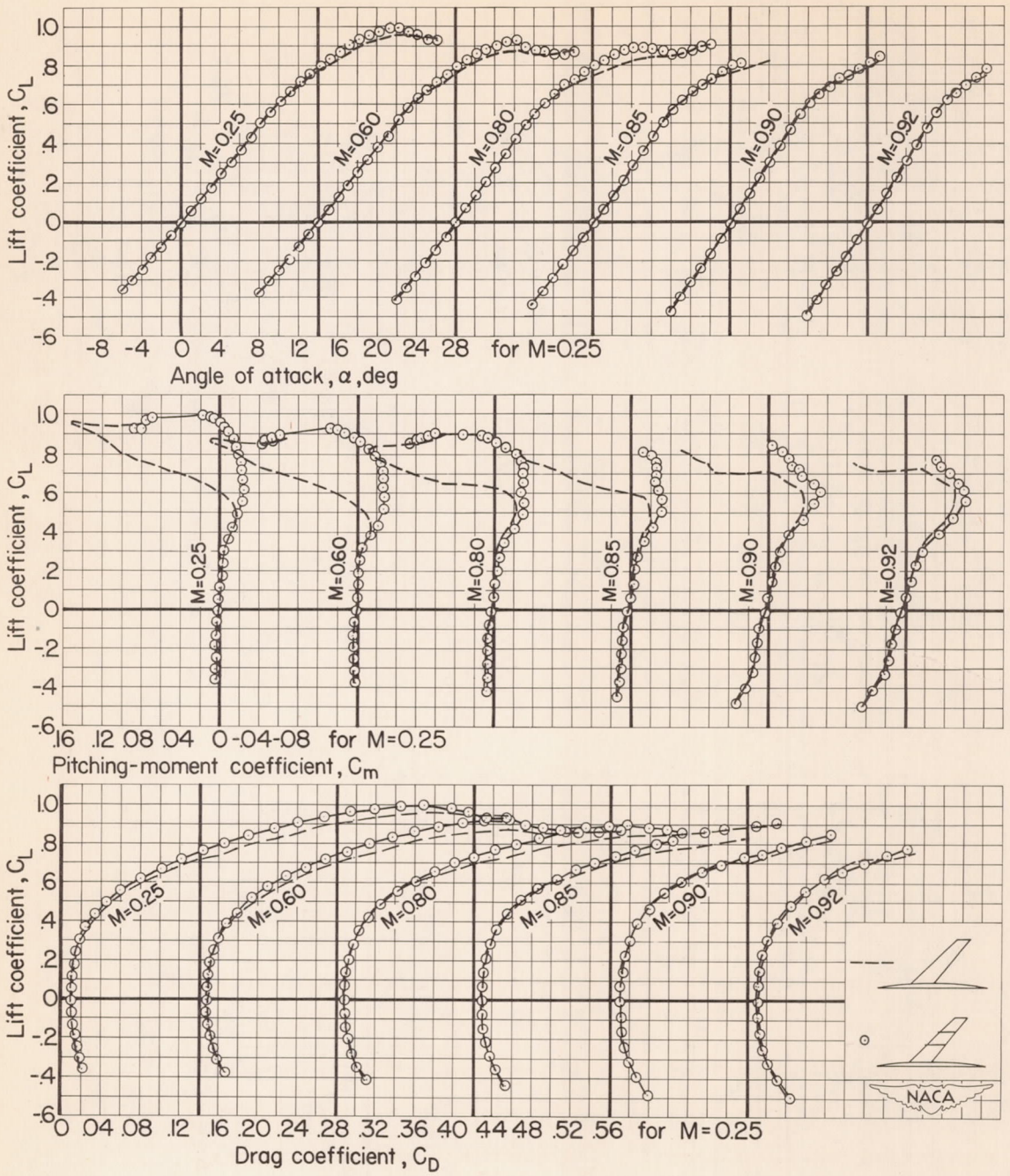

Figure 8.- The effect of fences at 0.44 and 0.69 semispan on the aerodynamic characteristics of the model with the tail off at various Mach numbers; R = 2,000,000.

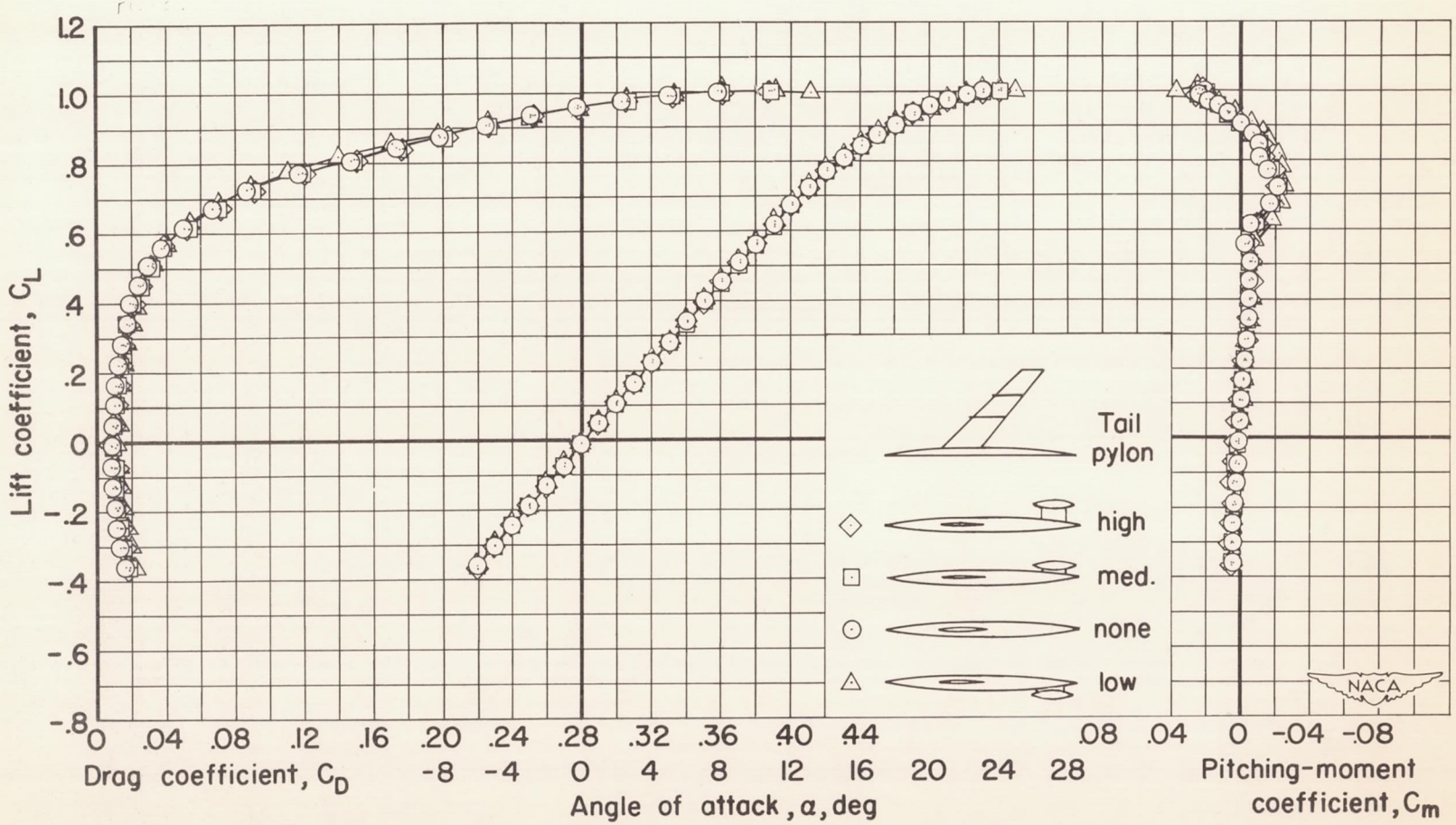

Figure 9.- The aerodynamic characteristics of the model with fences at 0.44 and 0.69 semispan, tail off, and with various tail support pylons at a Reynolds number of 10,000,000; M = 0.25.

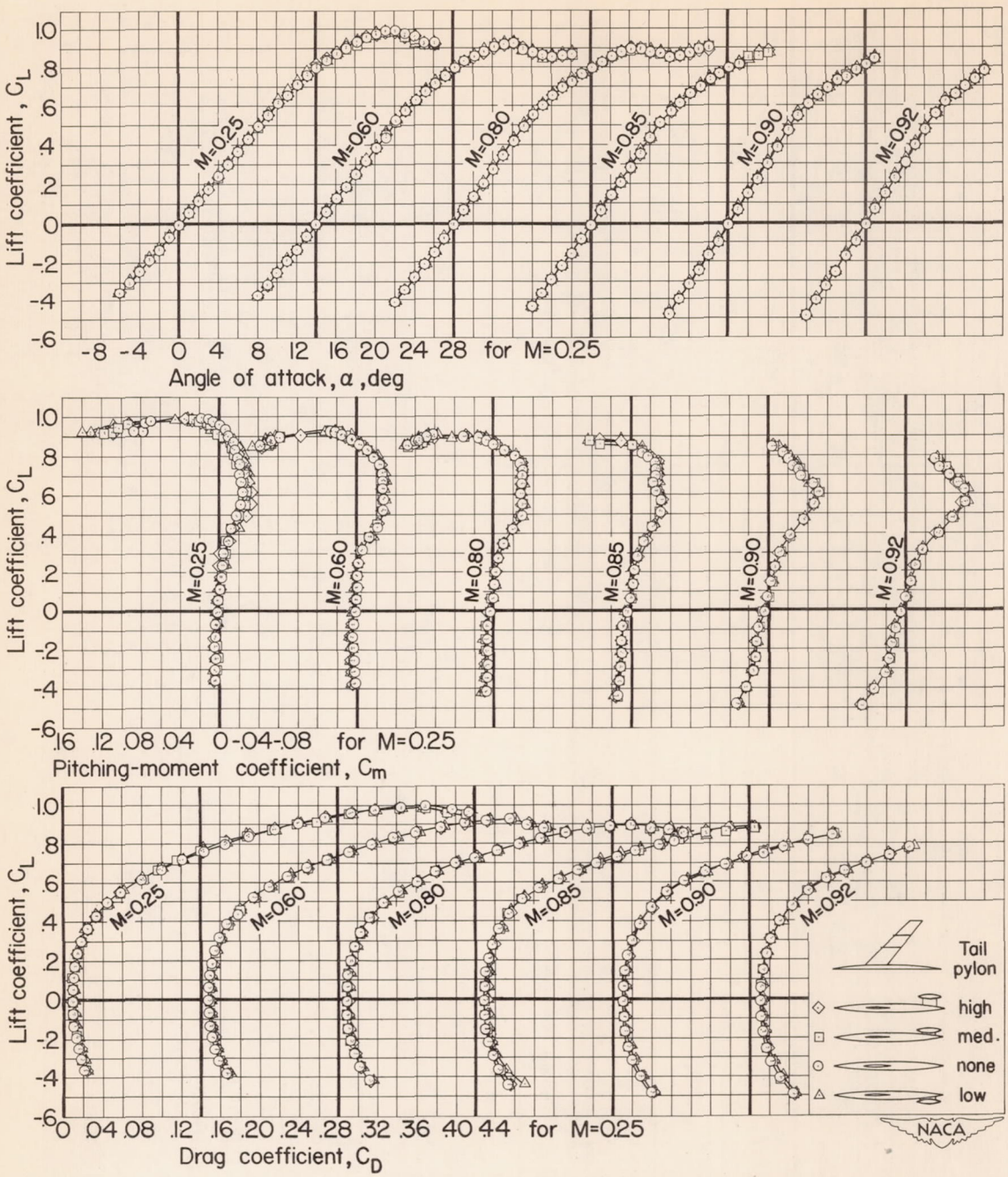

Figure 10.- The aerodynamic characteristics of the model with fences at 0.44 and 0.69 semispan, tail off, and with various tail support pylons at several Mach numbers; R = 2,000,000.

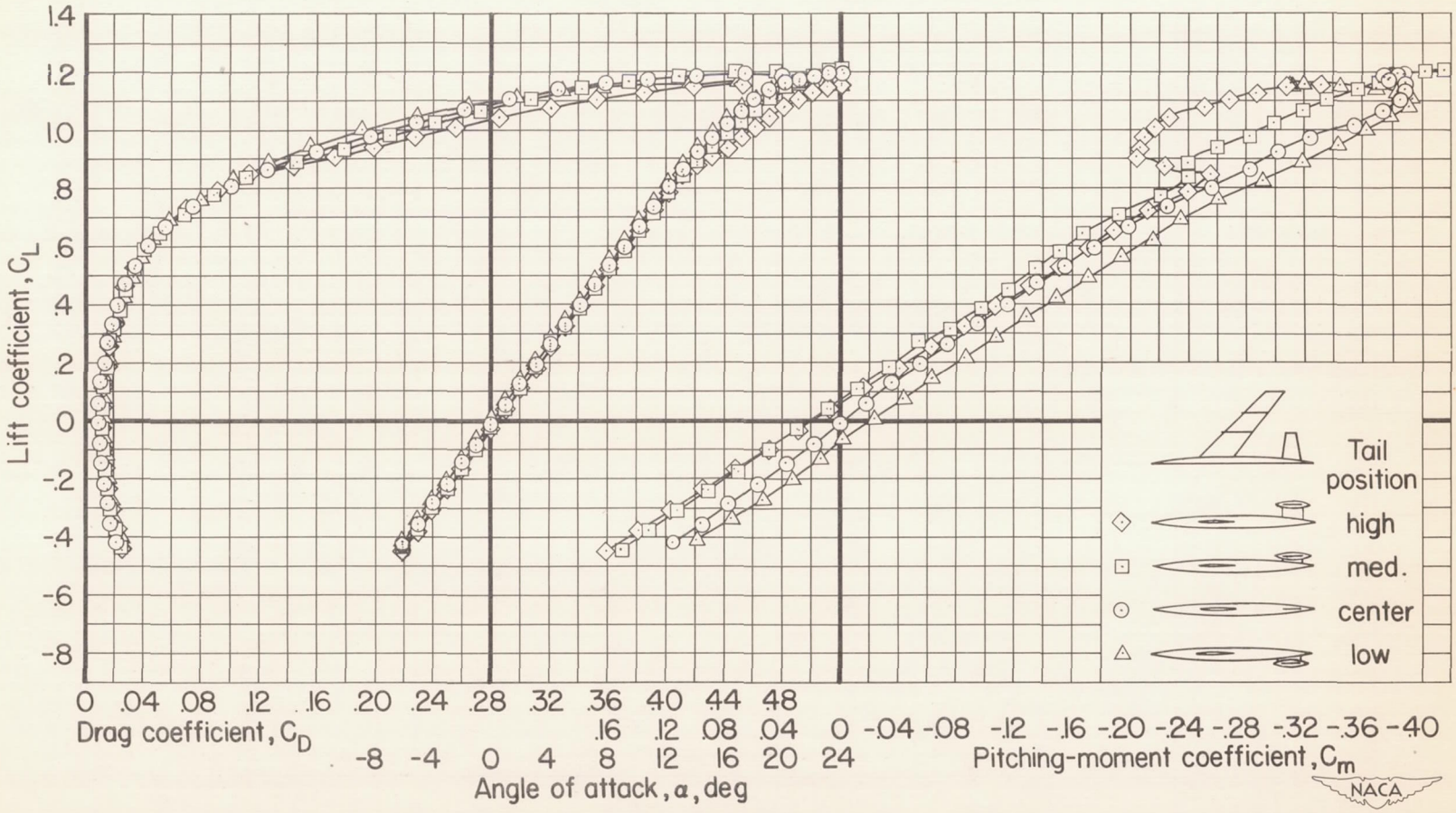

Figure 11.- The effect of tail height on the aerodynamic characteristics of the model with fences at 0.44 and 0.69 semispan at a Reynolds number of 10,000,000; M = 0.25.

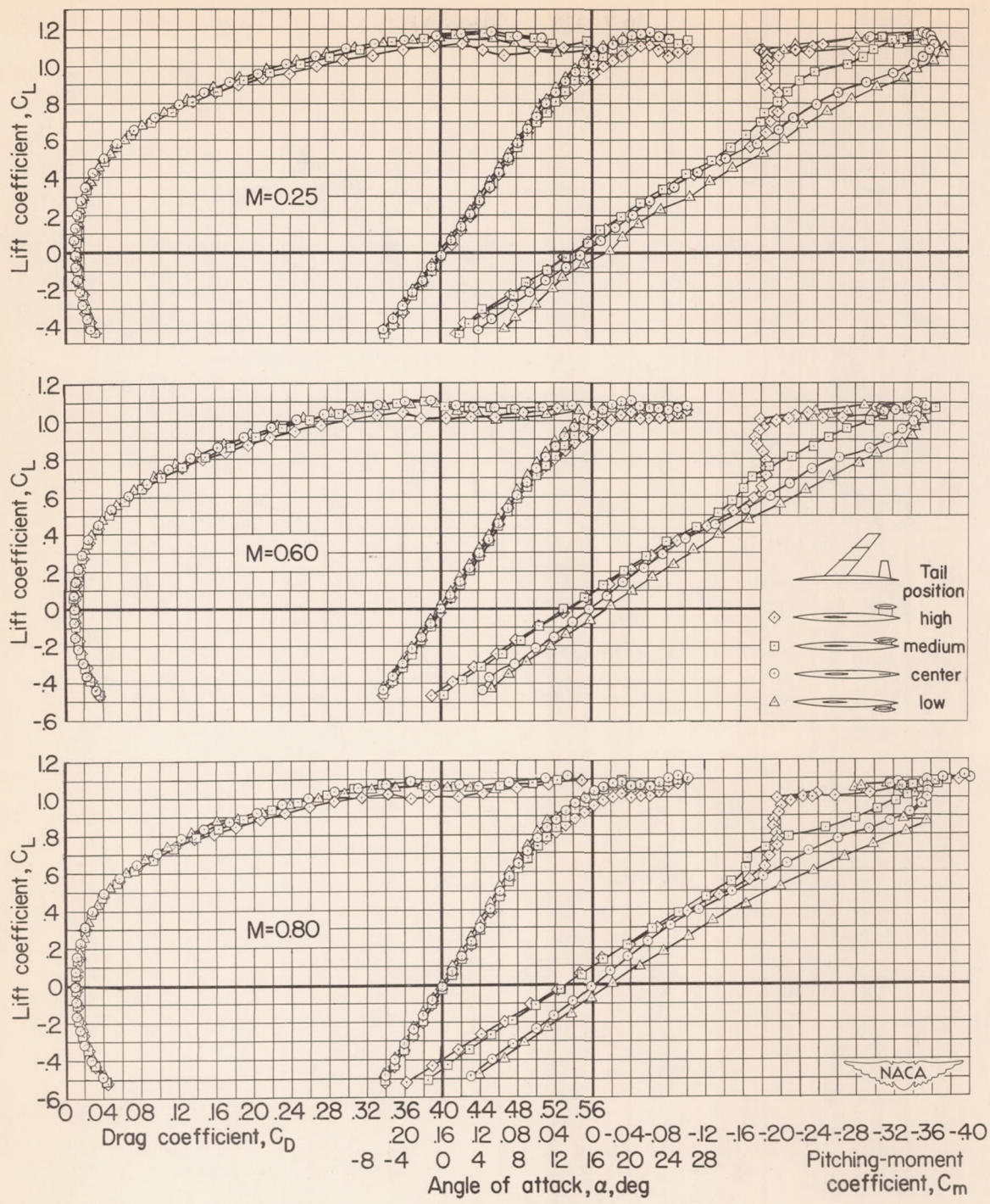

(a) M = 0.25, 0.60, and 0.80.

Figure 12.- The effect of tail height on the aerodynamic characteristics of the model with fences at 0.44 and 0.69 semispan at various Mach numbers; R = 2,000,000.

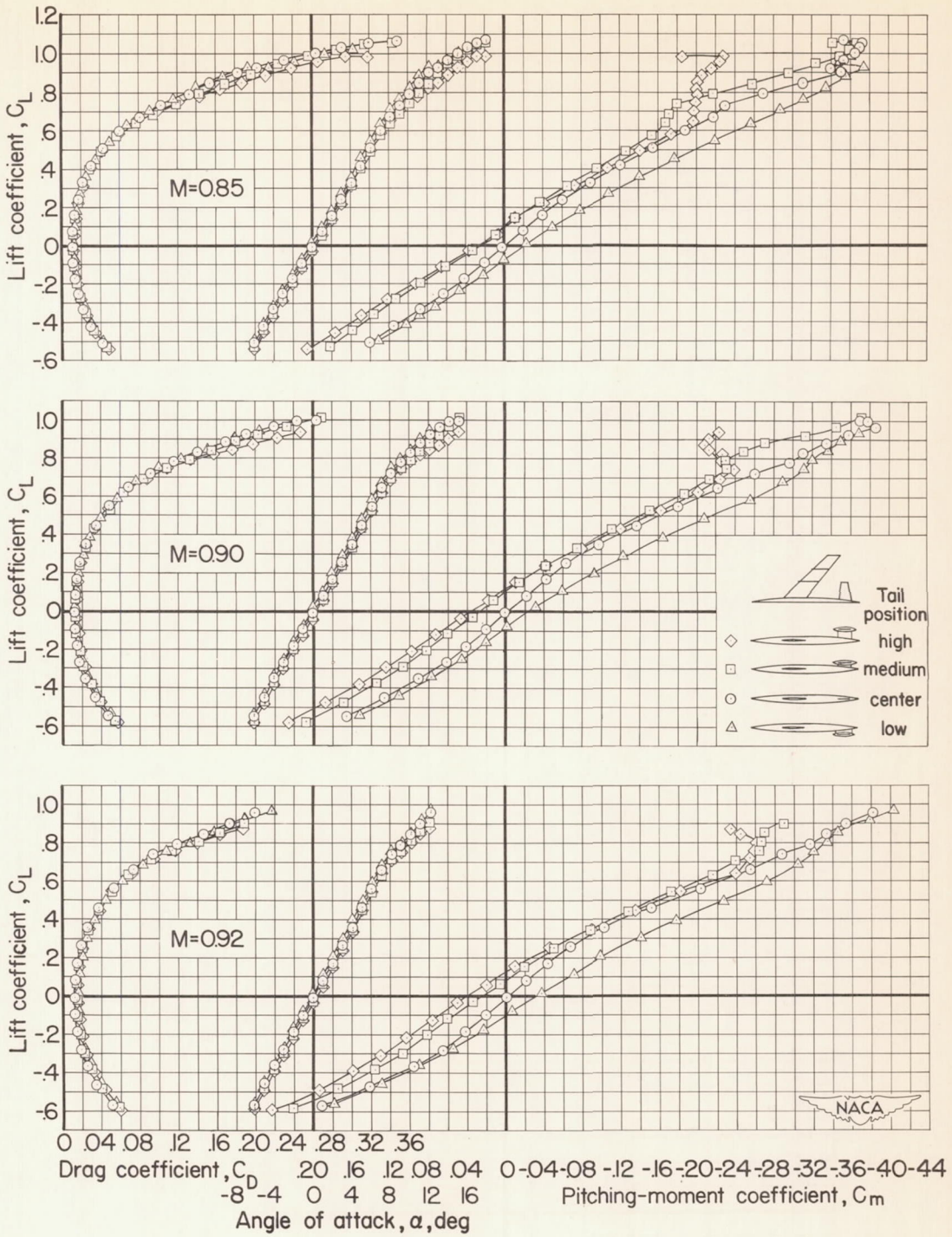

(b) M = 0.85, 0.90, and 0.92.

Figure 12.- Concluded.

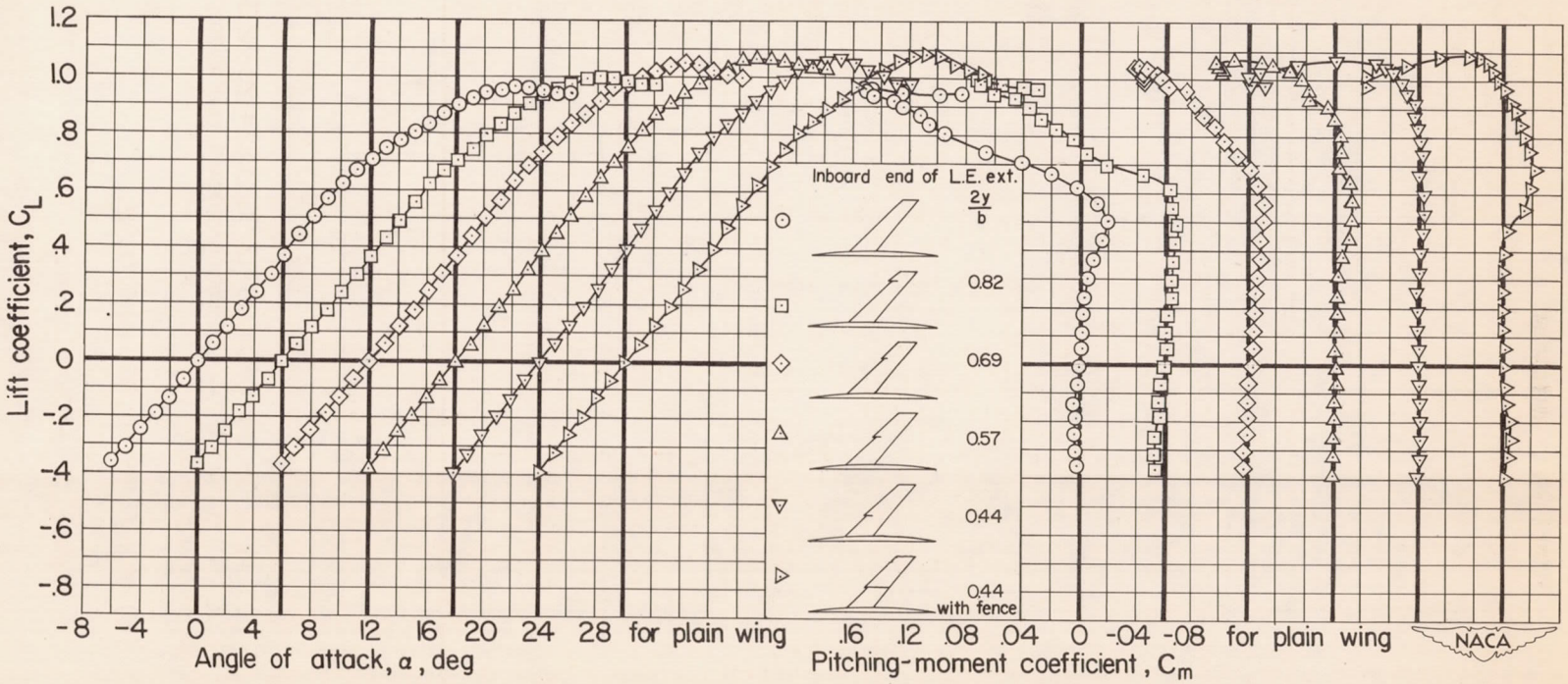

Figure 13.- Lift and pitching-moment characteristics of the model with the tail off and with various leading-edge extensions and a leading-edge extension-fence combination at a Mach number of 0.25; R = 2,000,000.

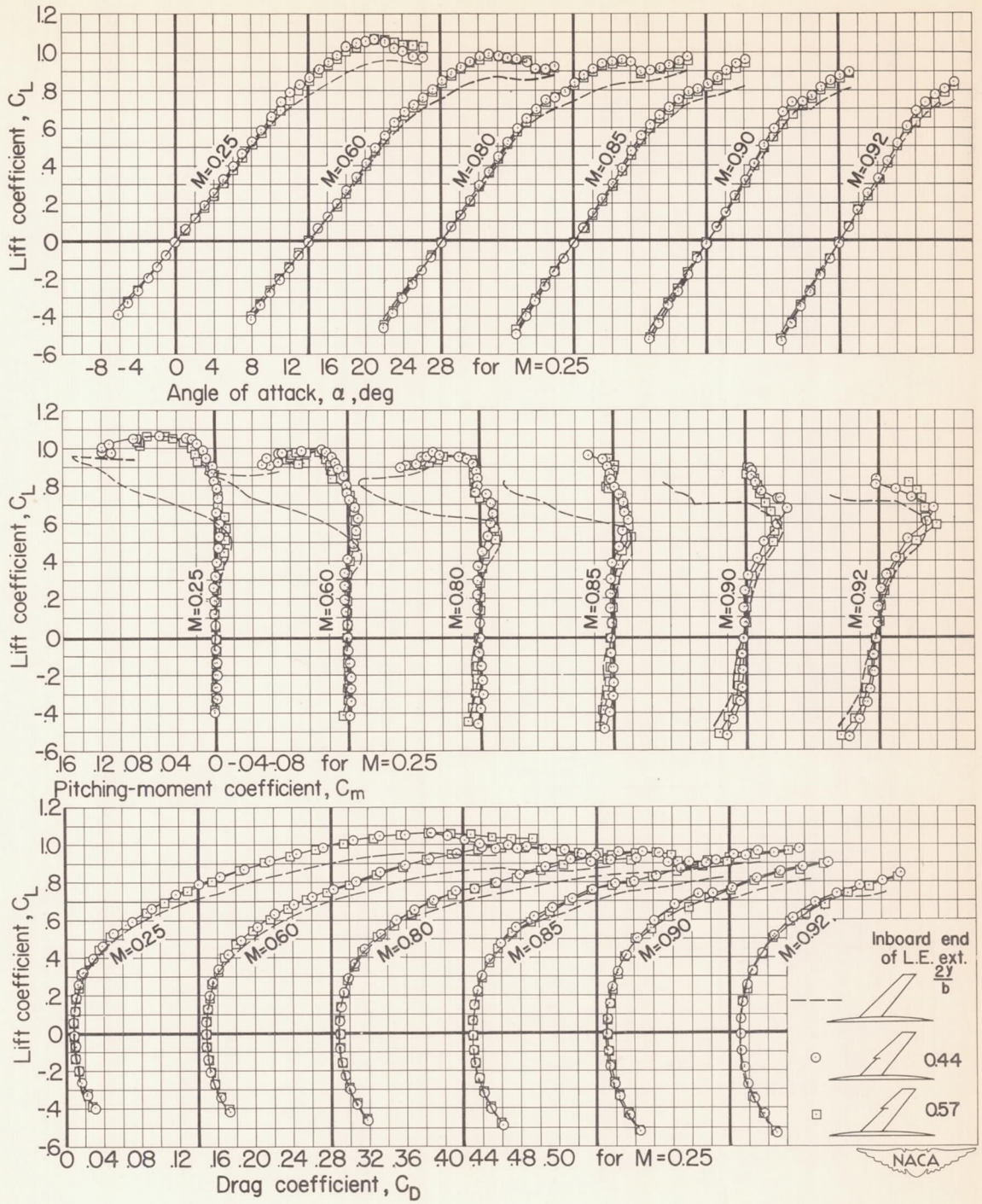

Figure 14.- The effect of leading-edge extensions on the aerodynamic characteristics of the model with tail off at various Mach numbers.

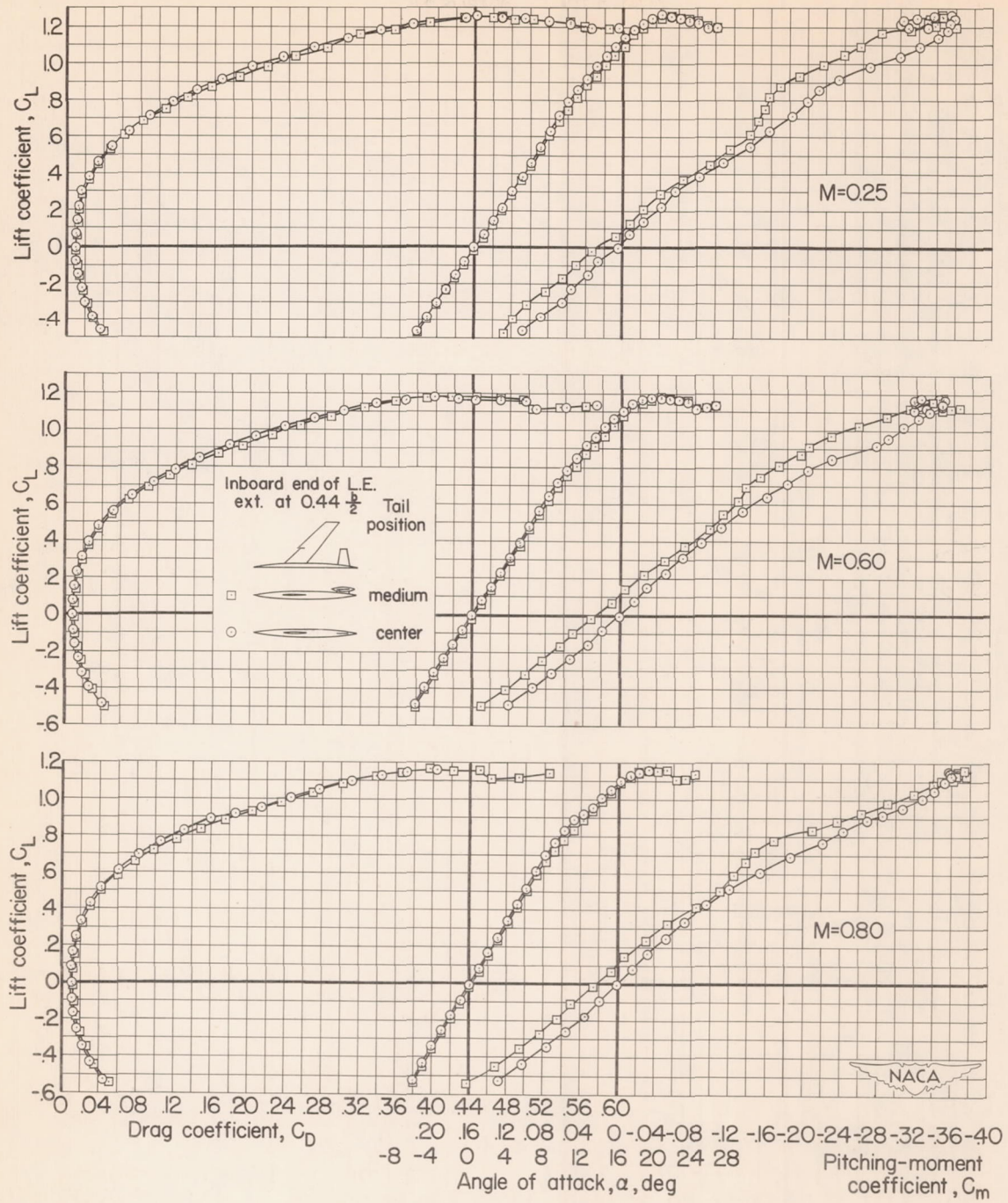

(a) M = 0.25, 0.60, and 0.80.

Figure 15.- The effect of tail height on the model with a leading-edge extension between the tip and 0.44 semispan at various Mach numbers; R = 2,000,000.

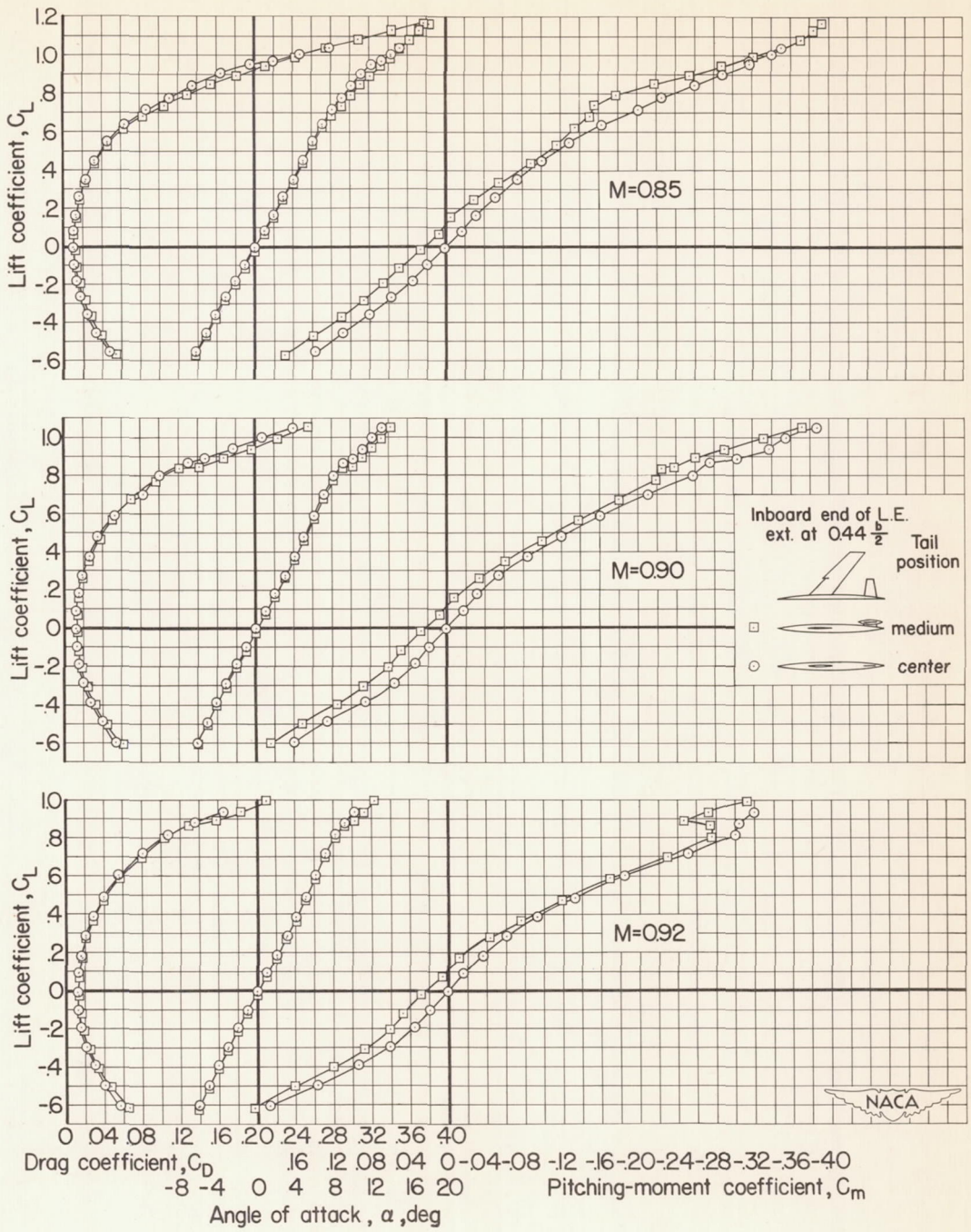

(b) M = 0.85, 0.90, and 0.92.

Figure 15.- Concluded.

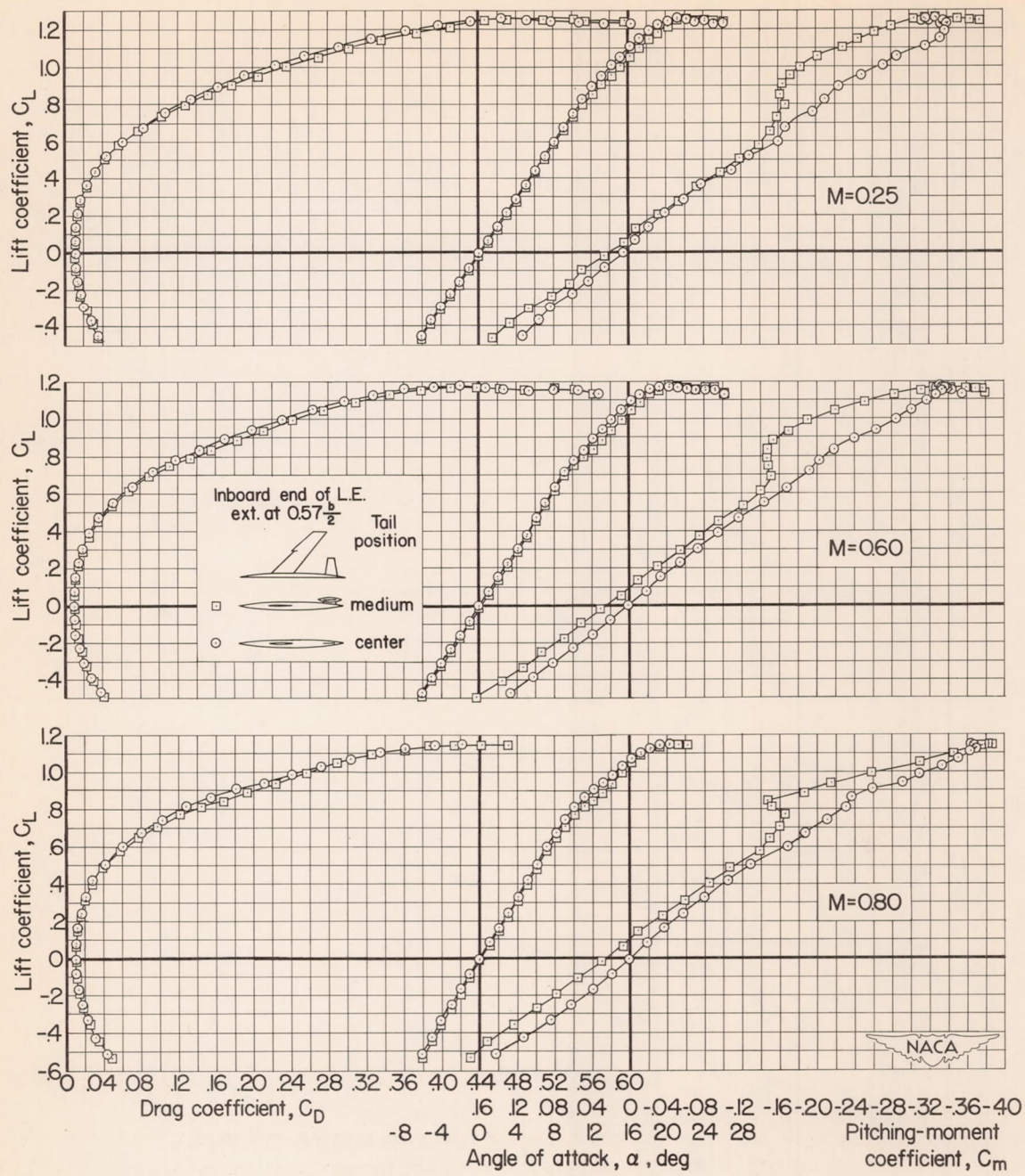

(a) M = 0.25, 0.60, and 0.80.

Figure 16.- The effect of tail height on the model with a leading-edge extension between the tip and 0.57 semispan at various Mach numbers; R = 2,000,000.

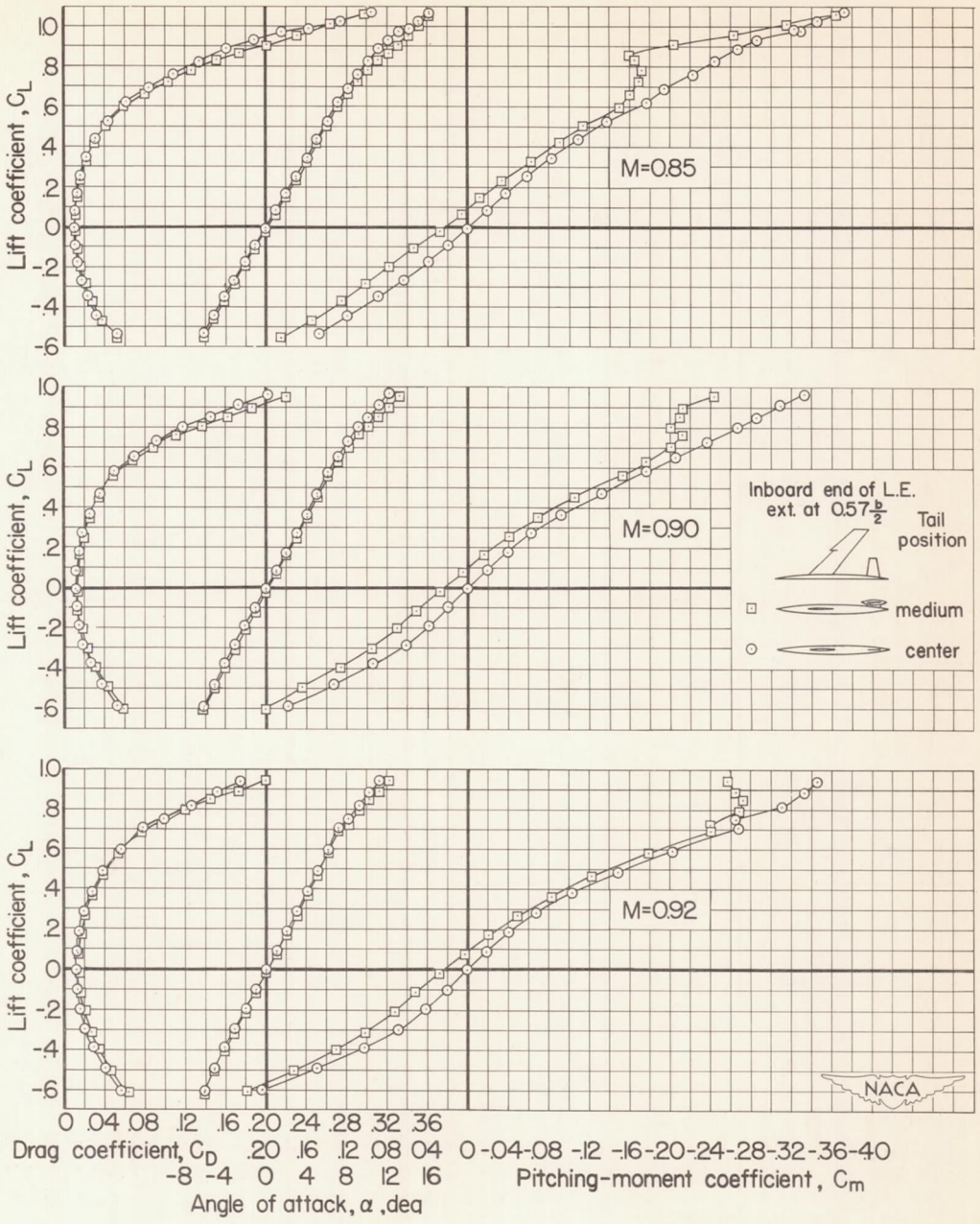

(b) M = 0.85, 0.90, and 0.92.

Figure 16.- Concluded.

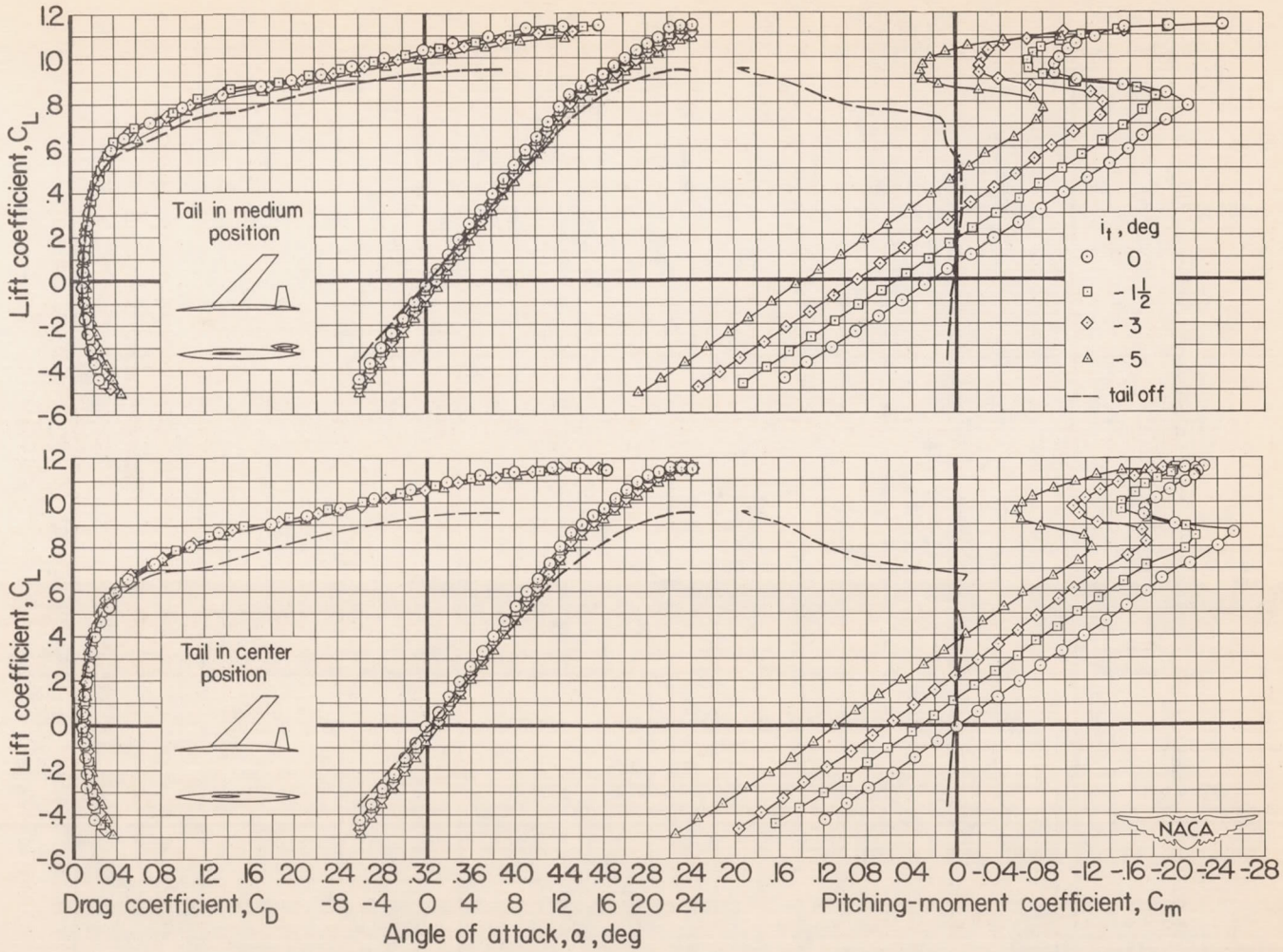

Figure 17.- The aerodynamic characteristics of the model with the tail in the medium and center positions at a Reynolds number of 10,000,000; M = 0.25.

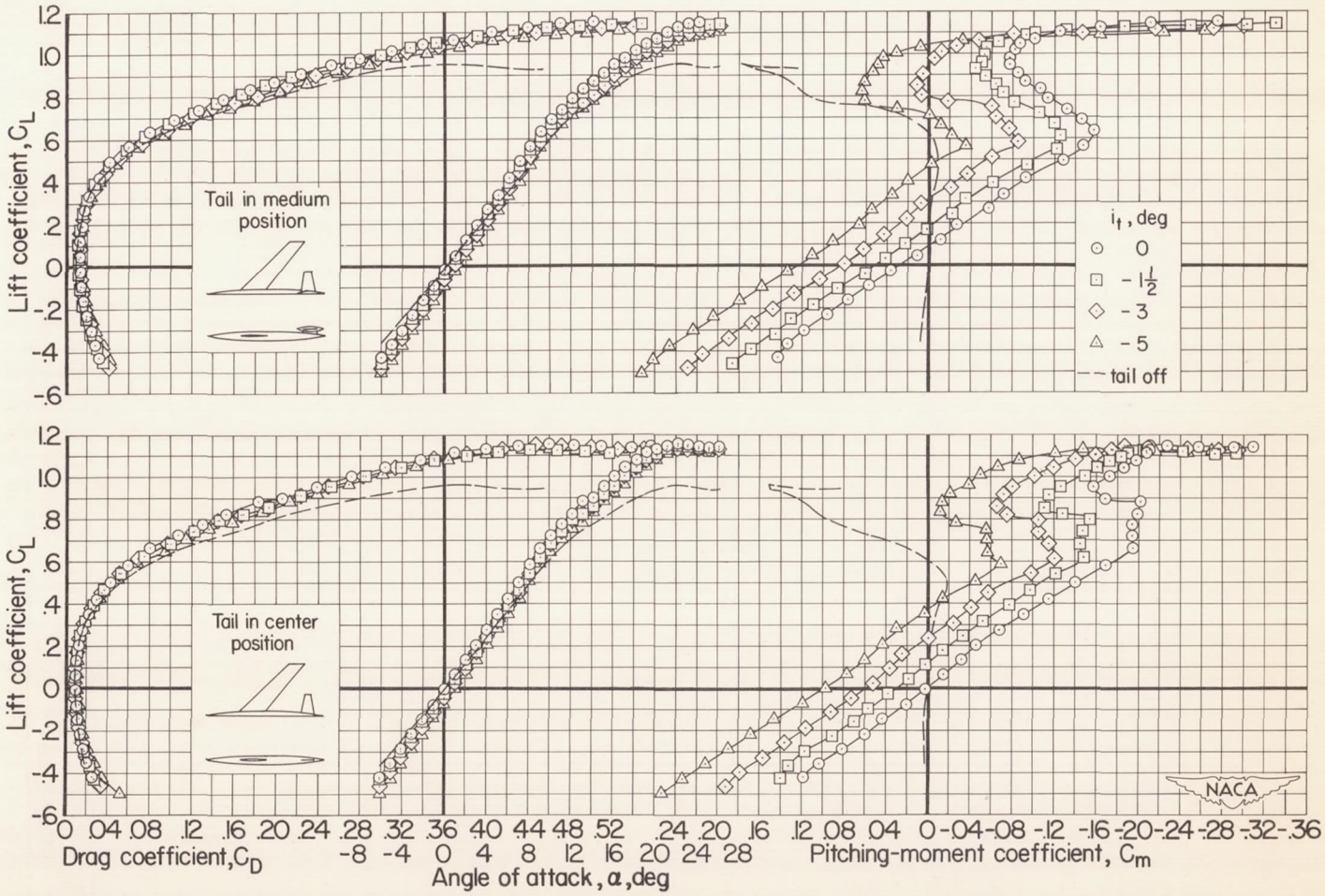

(a) M = 0.25

Figure 18.- The aerodynamic characteristics of the model with the tail in the medium and center positions at a Reynolds number of 2,000,000.

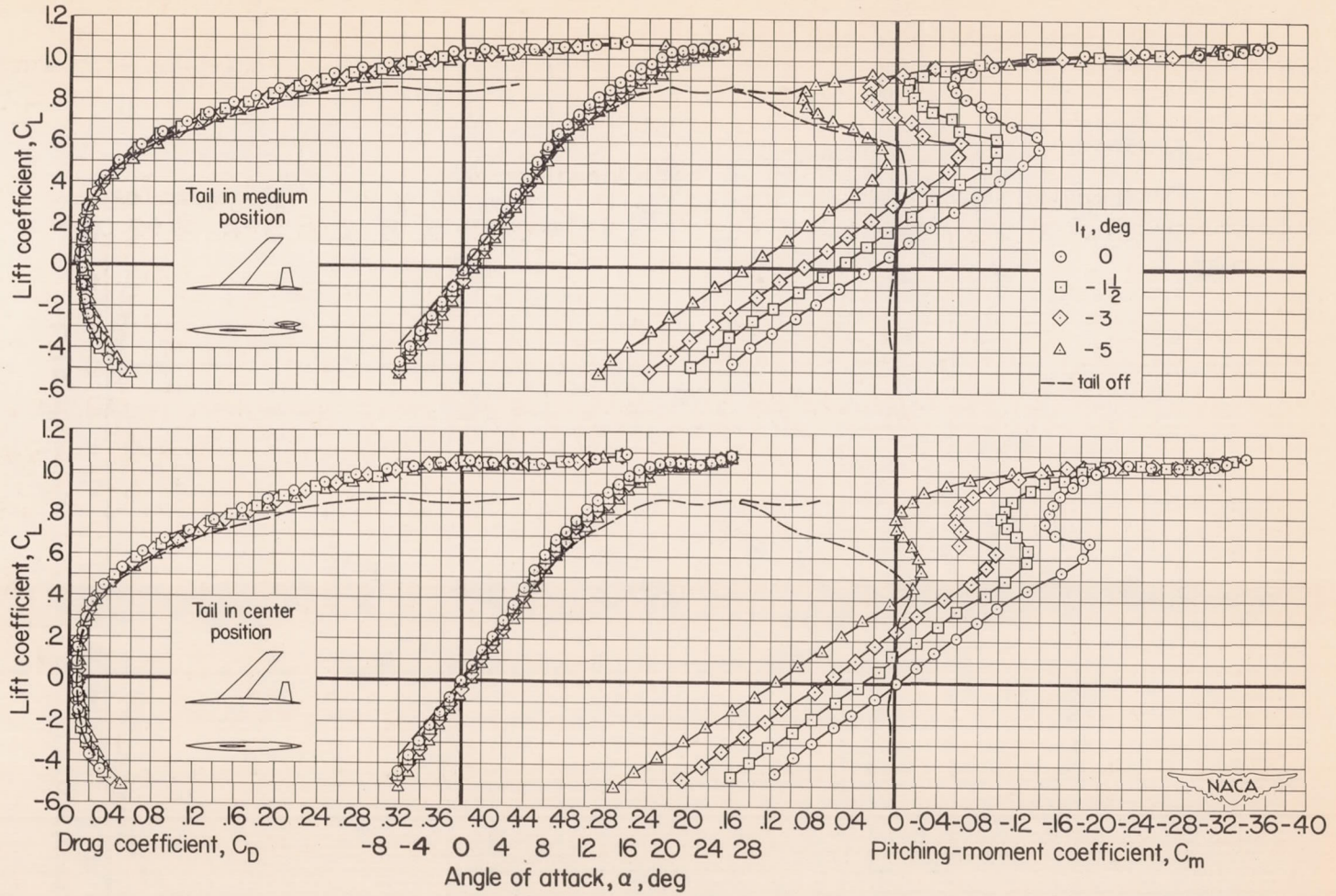

(b) M = 0.60

Figure 18.- Continued.

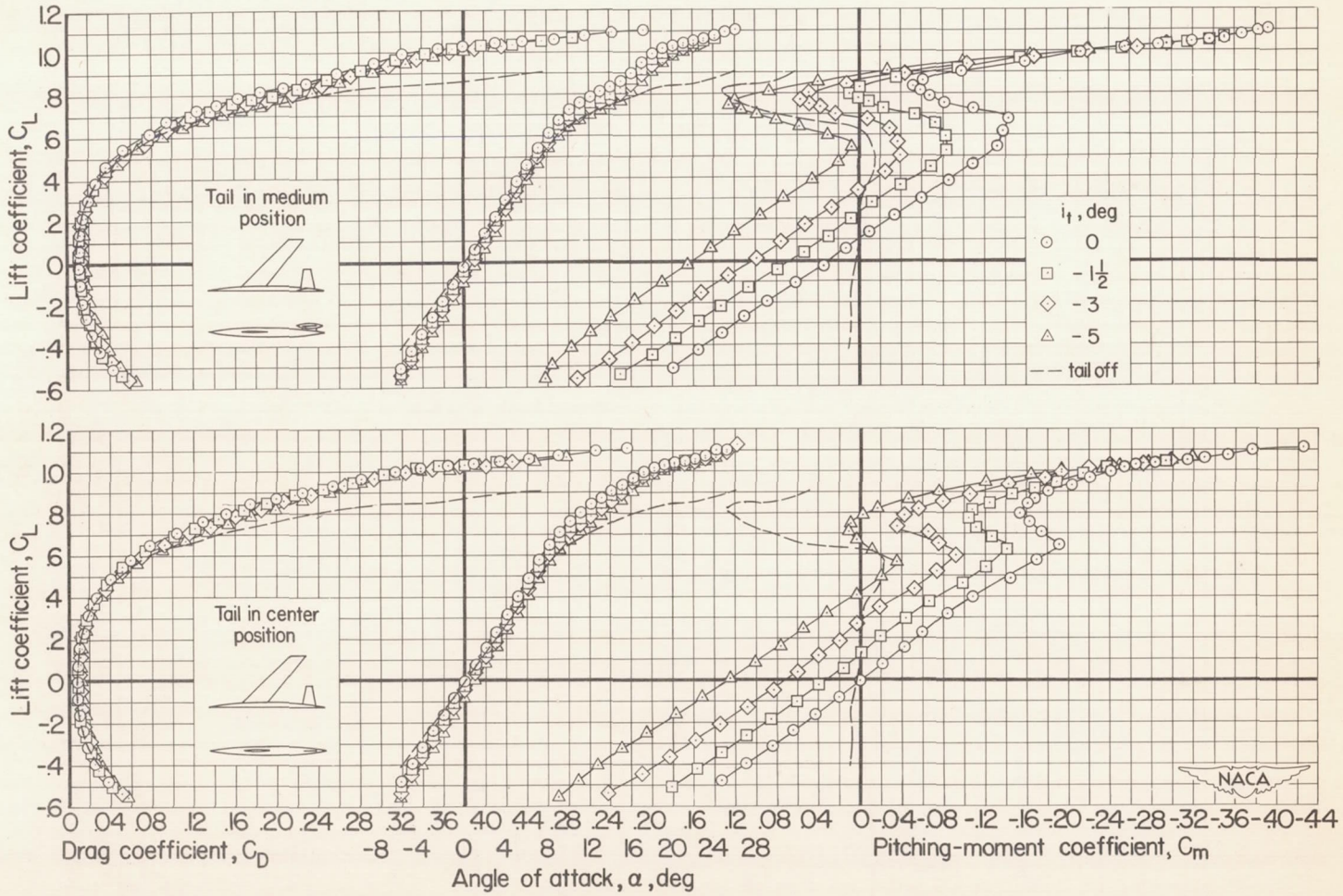

(c) M = 0.80

Figure 18.- Continued.

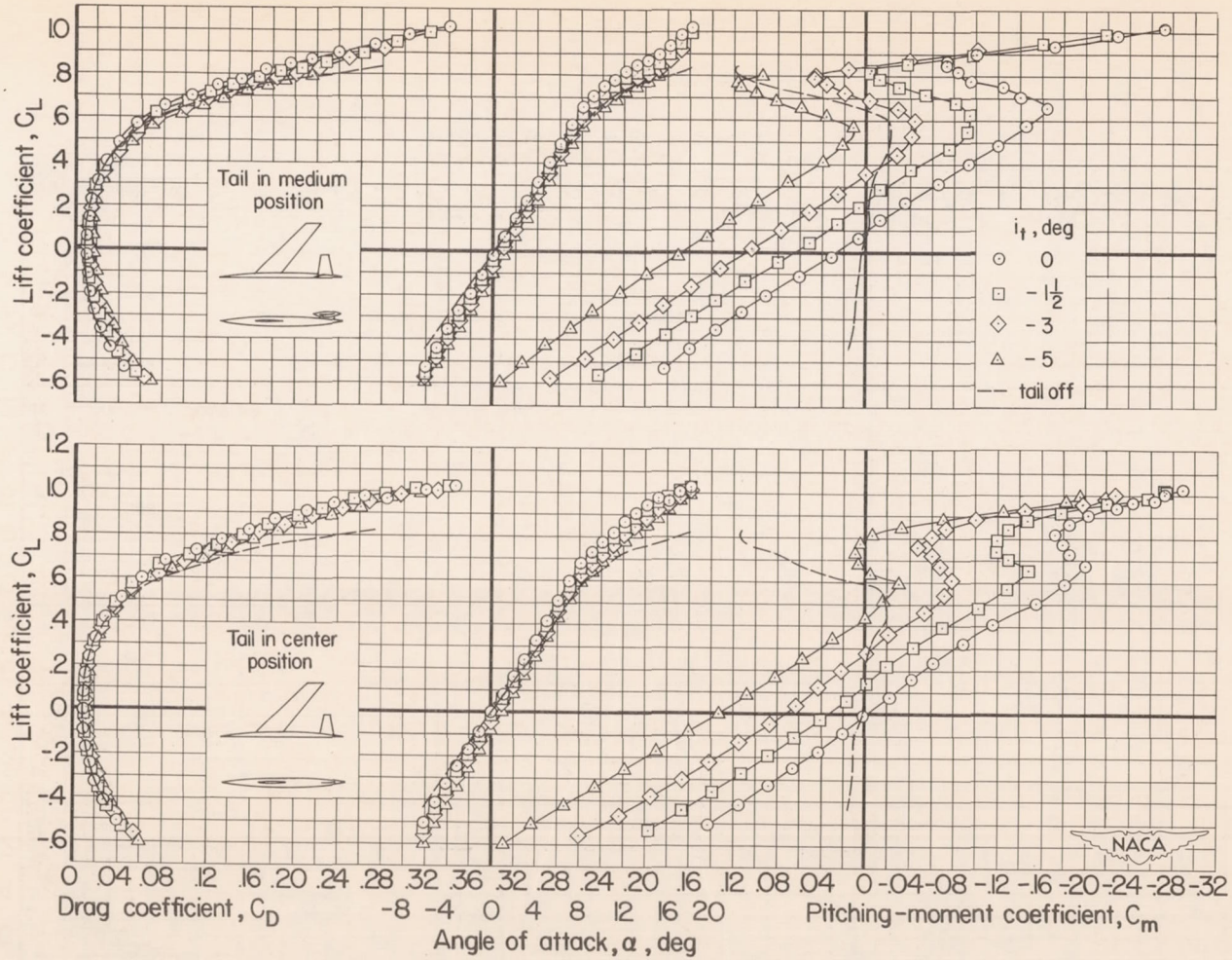

(d) M = 0.85

Figure 18.- Continued.

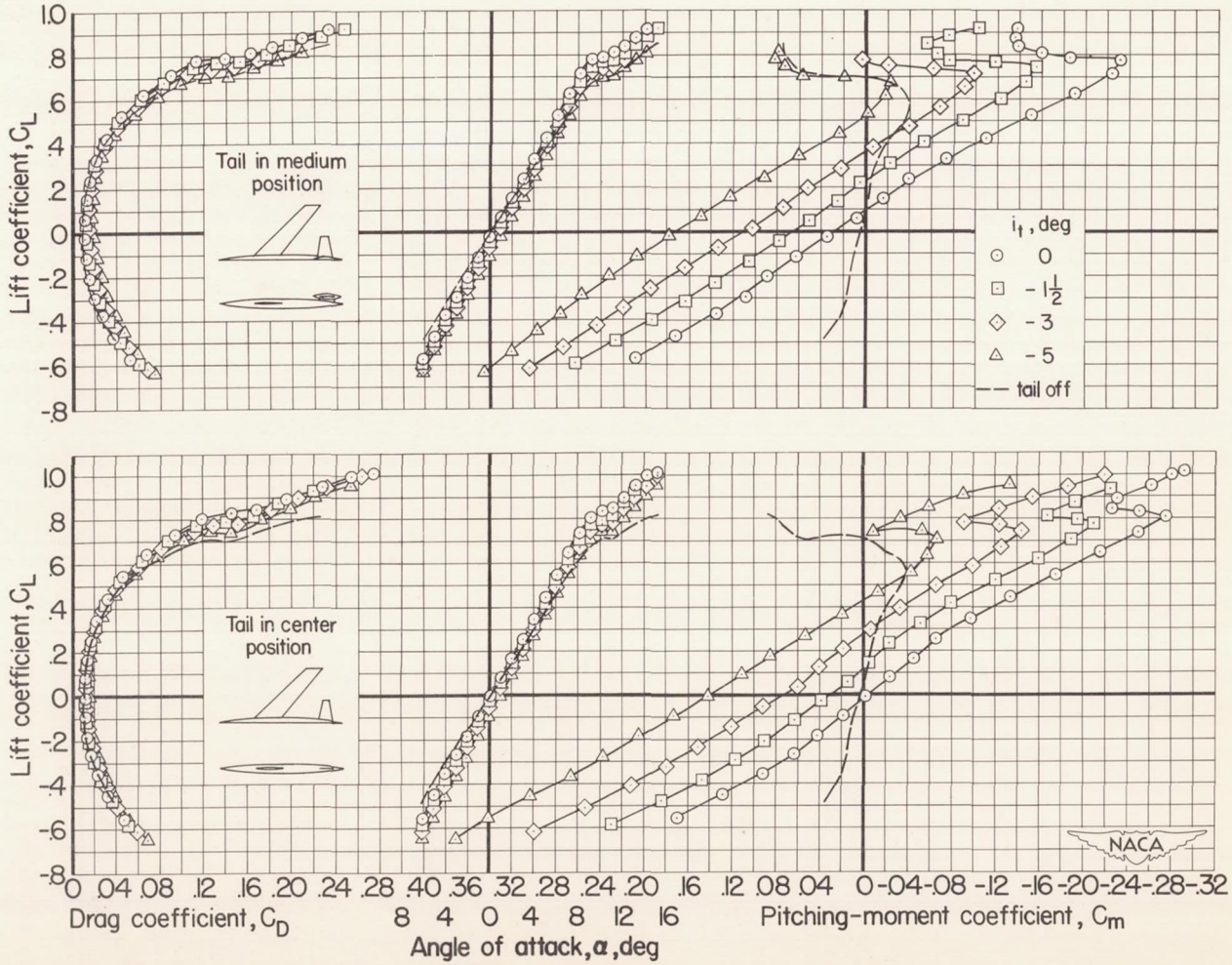

(e) M = 0.90

Figure 18.- Continued.

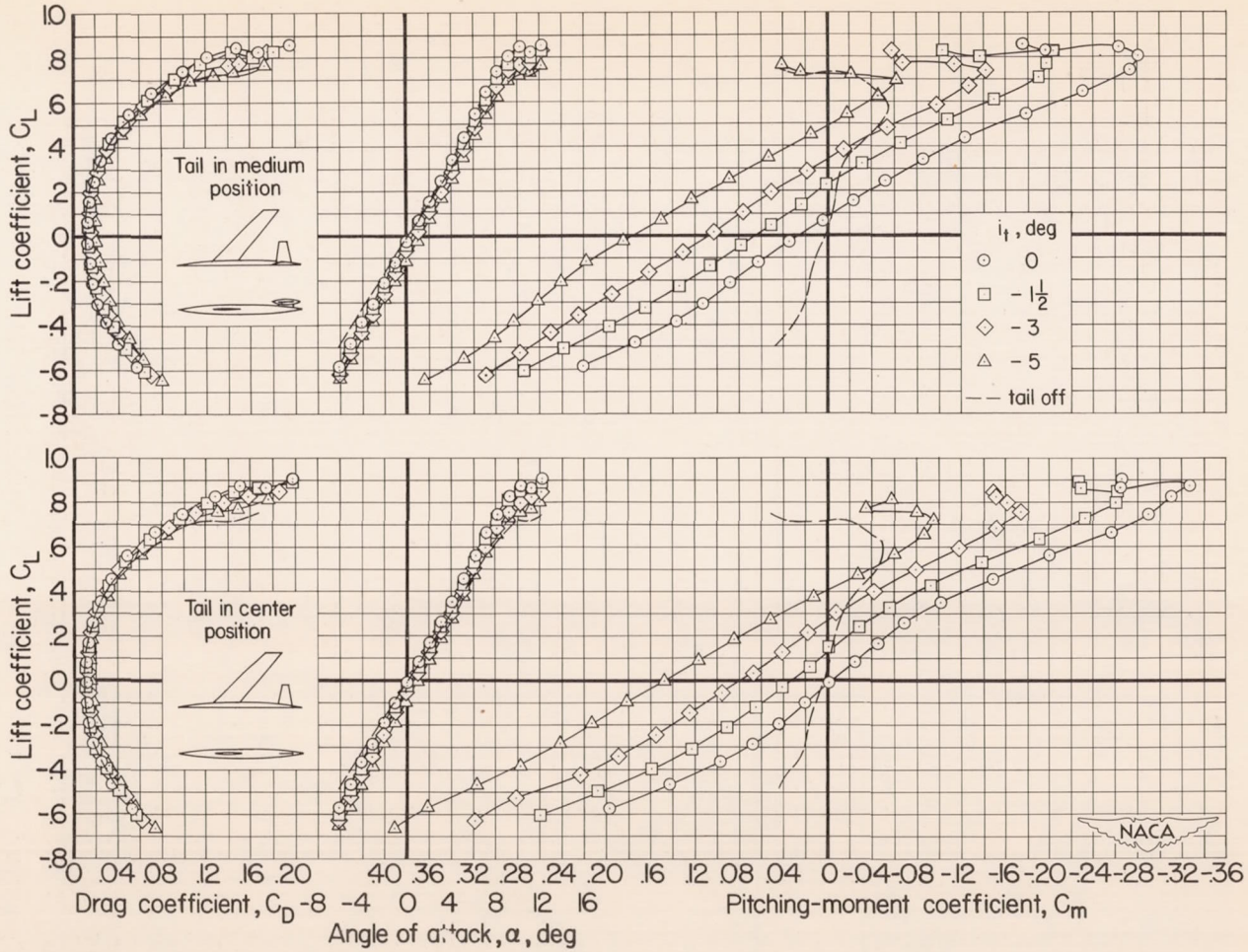

(f) M = 0.92

Figure 18.- Concluded.

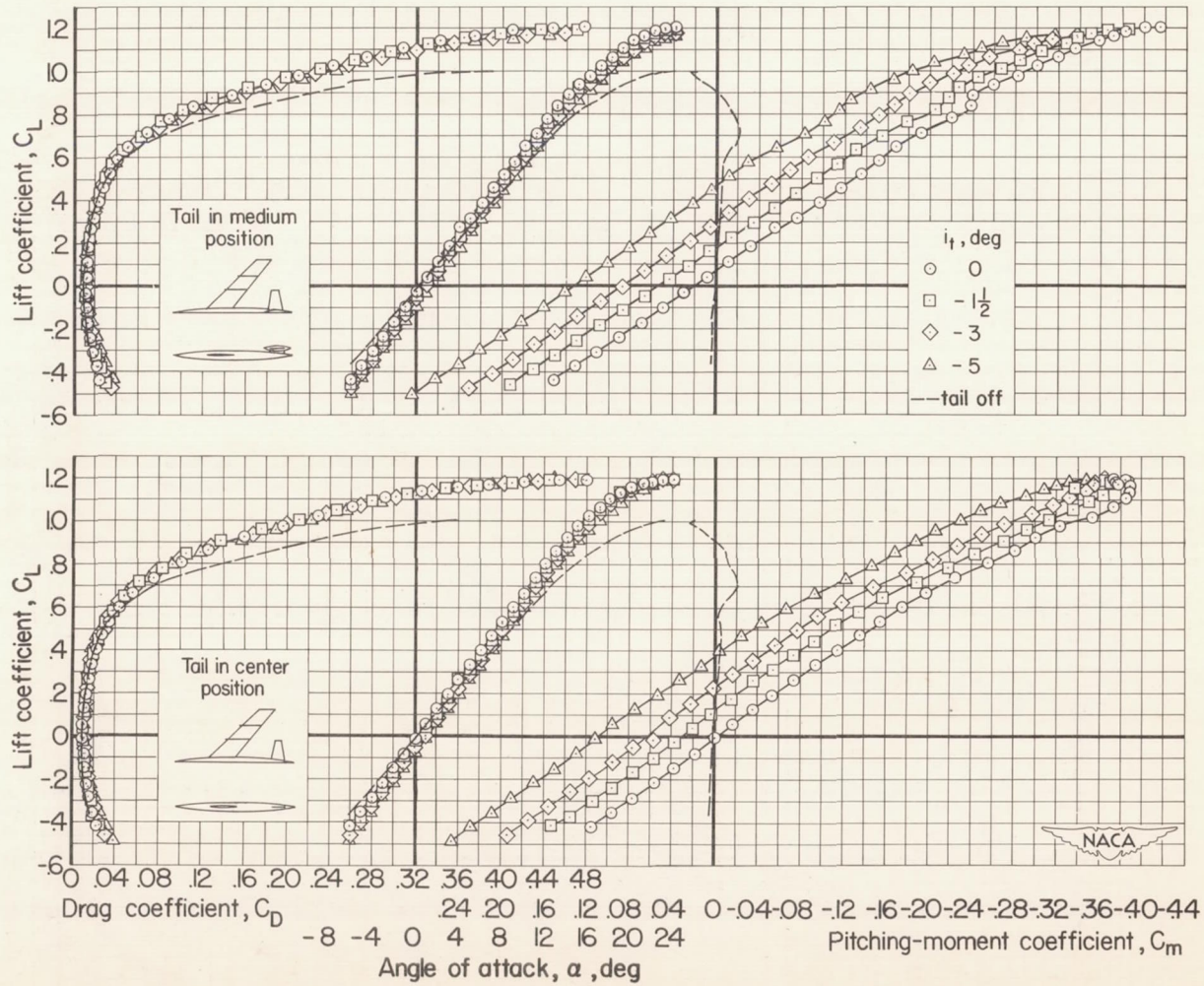

Figure 19.- The aerodynamic characteristics of the model with fences and the tail in the medium and center positions at a Reynolds number of 10,000,000; M = 0.25.

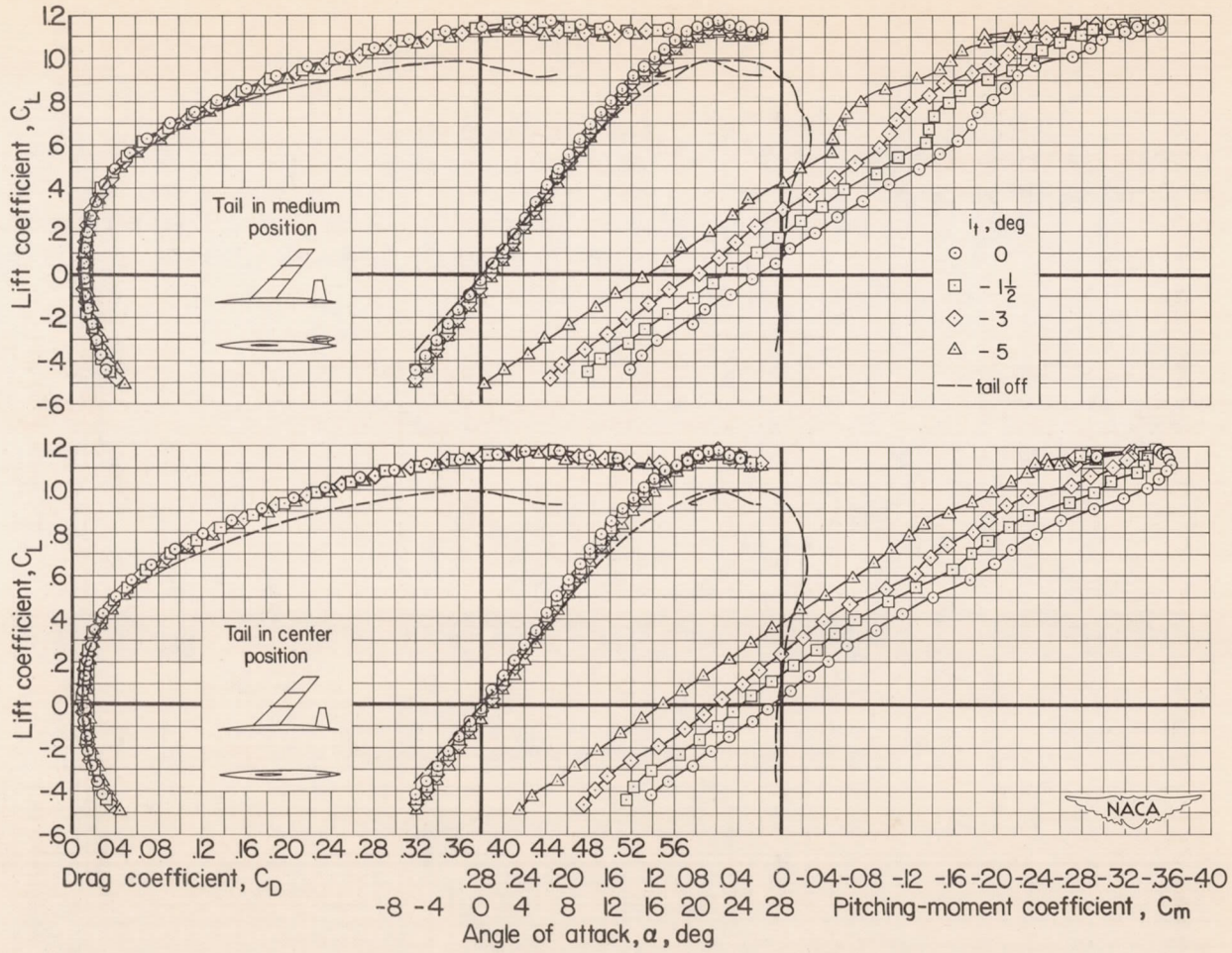

(a) M = 0.25

Figure 20.- The aerodynamic characteristics of the model with fences and the tail in the medium and center positions at a Reynolds number of 2,000,000.

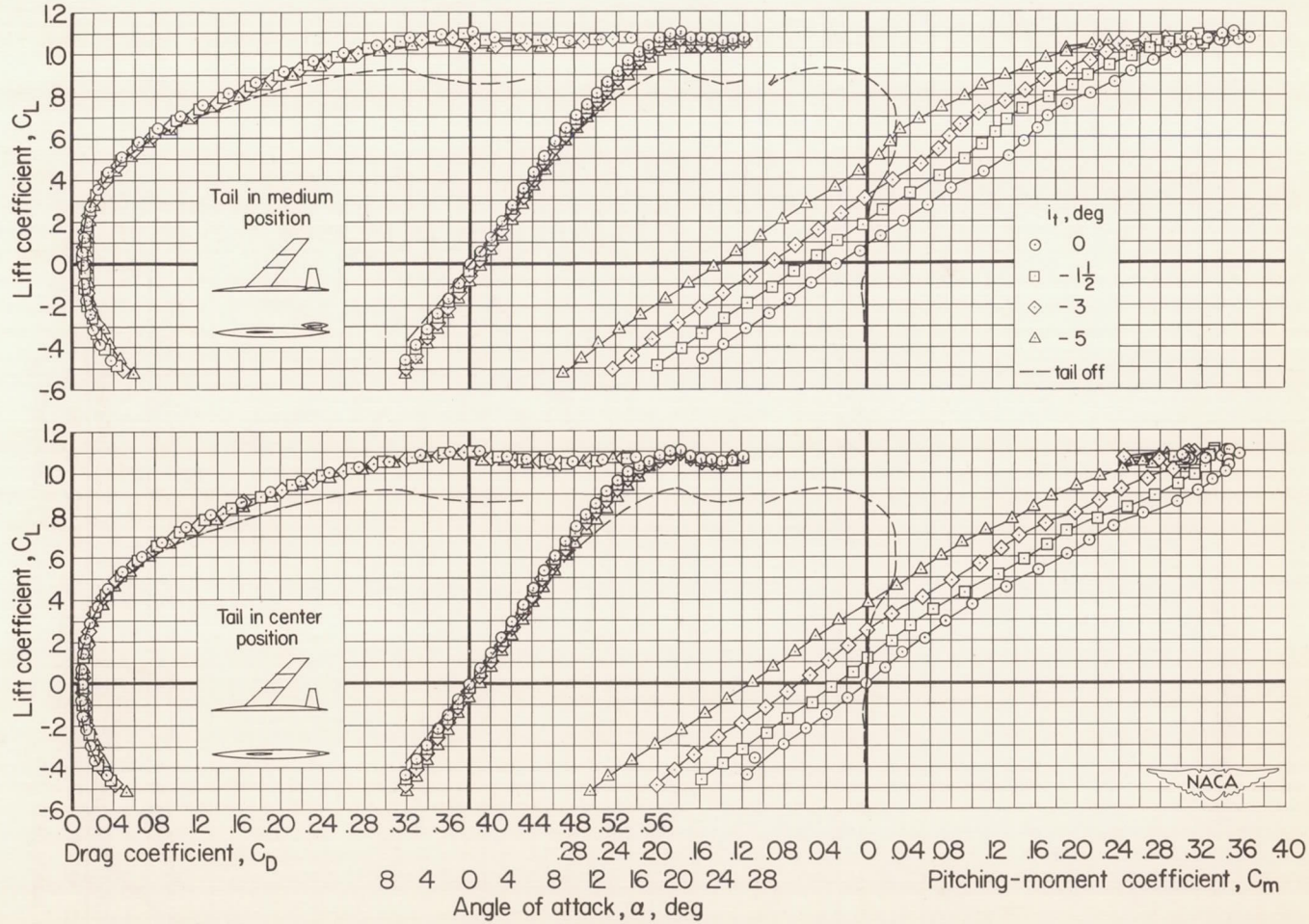

(b) M = 0.60

Figure 20.- Continued.

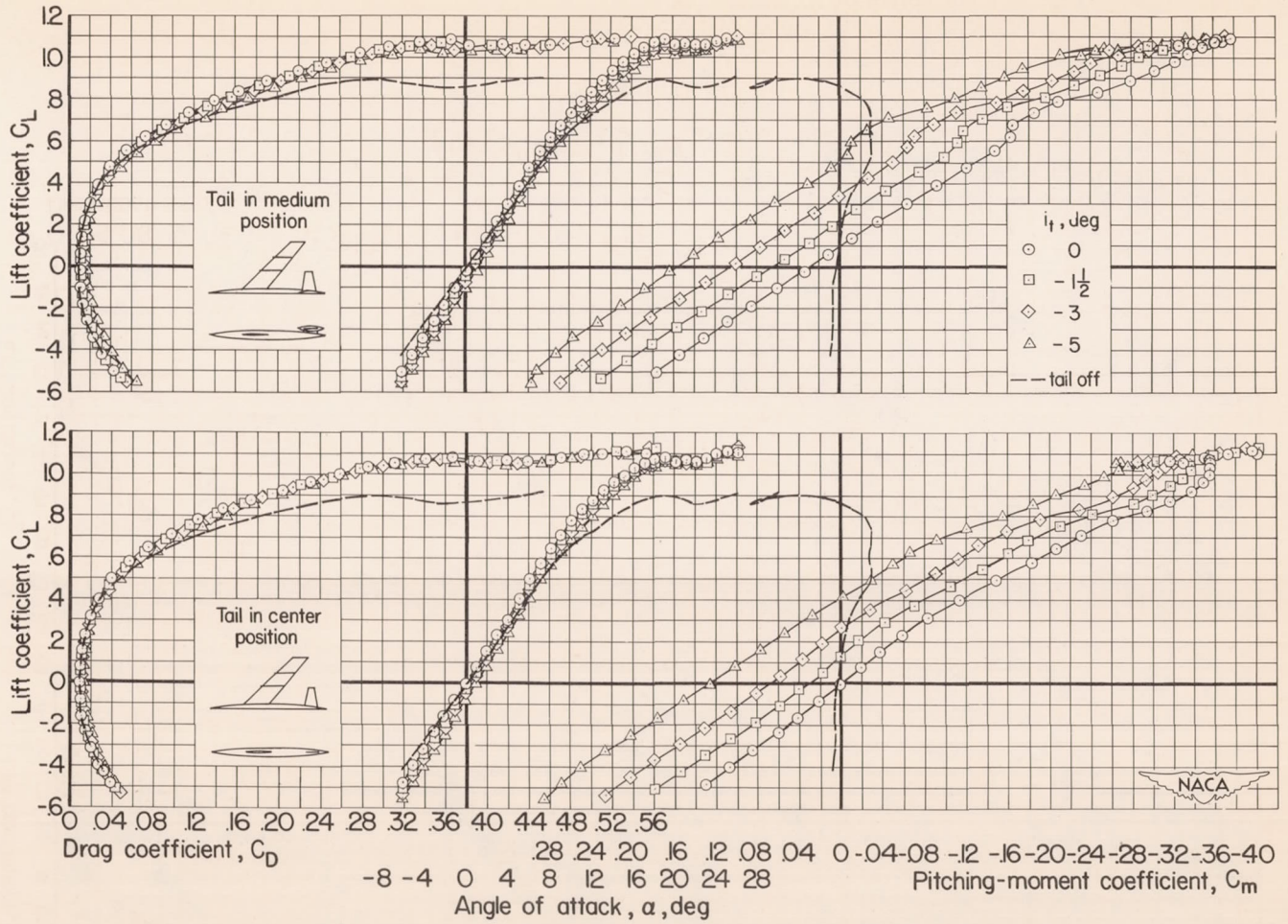

(c) M = 0.80

Figure 20.- Continued.

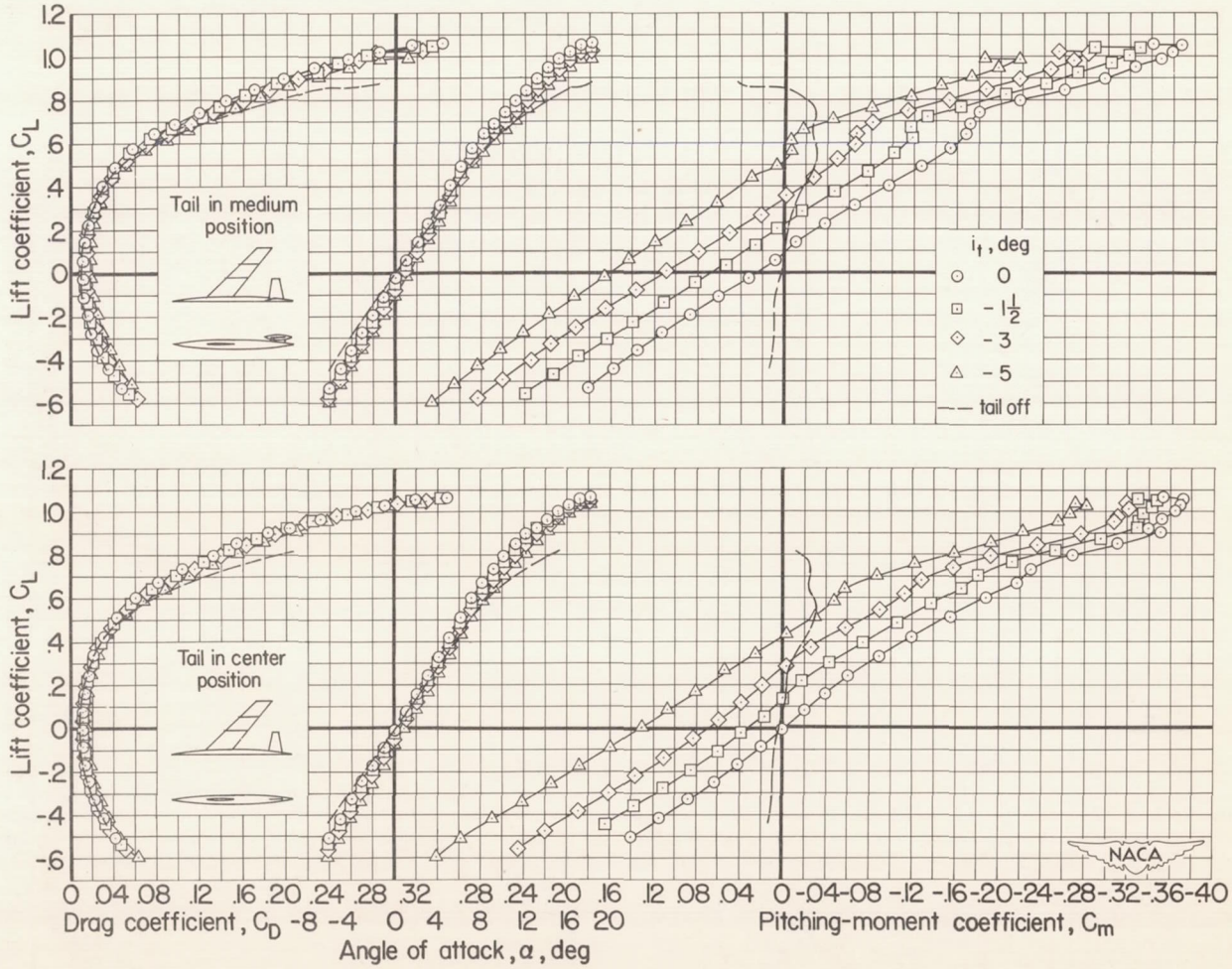

(d) M = 0.85

Figure 20.- Continued.

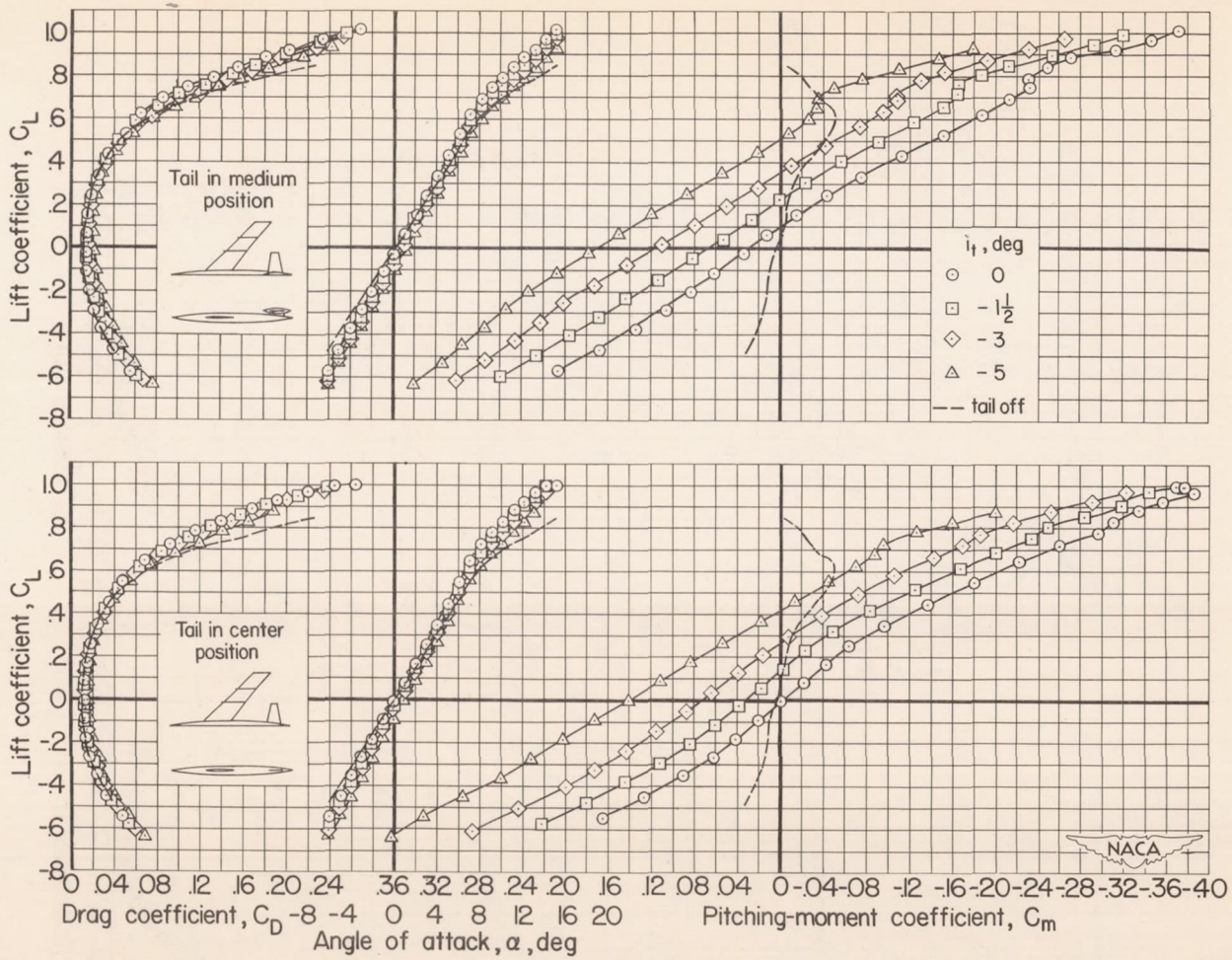

(e) M = 0.90

Figure 20.- Continued.

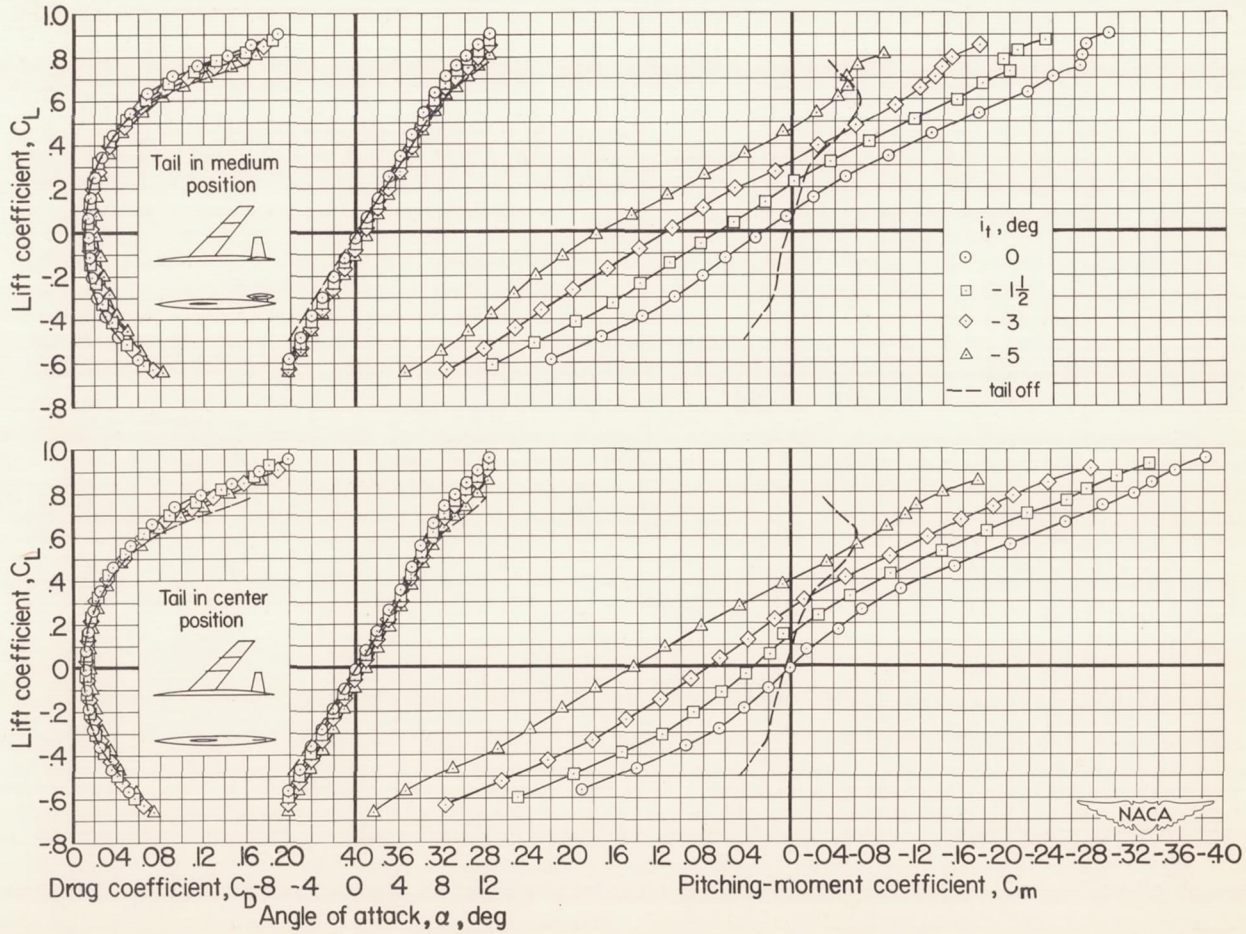

(f) M = 0.92

Figure 20.- Concluded.

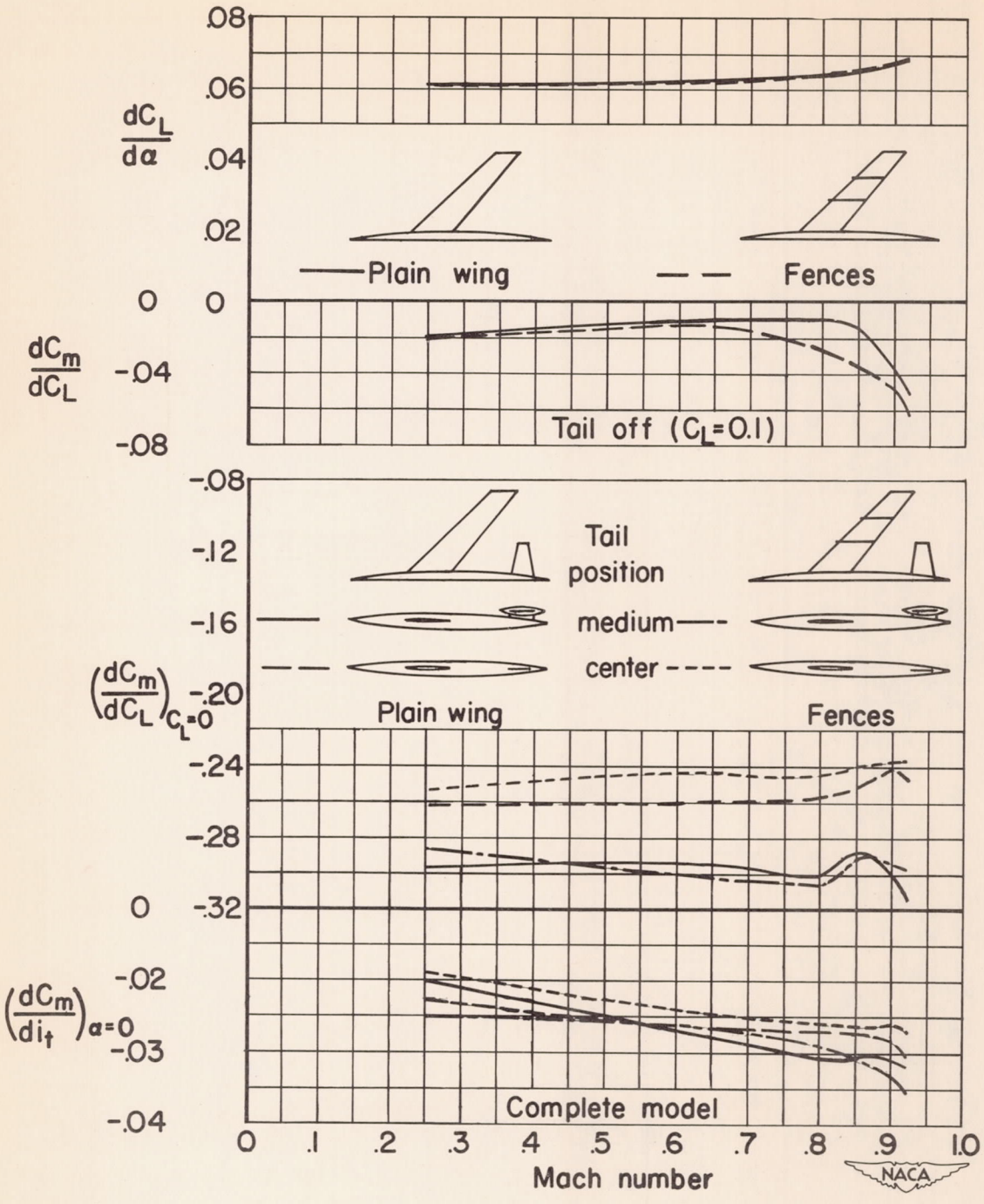

Figure 21.- The variation with Mach number of lift-curve slope, pitching-moment-curve slope, and stabilizer effectiveness; R = 2,000,000.

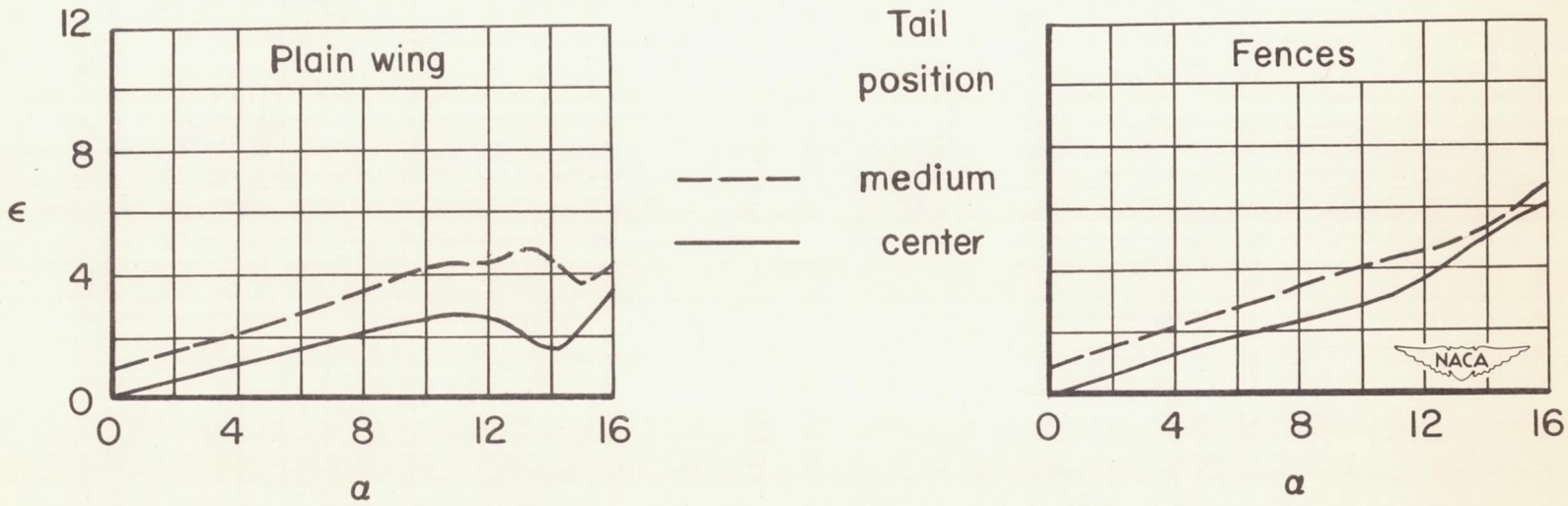

Figure 22.- The variation of effective downwash at the tail with angle of attack for the model with and without fences at a Reynolds number of 10,000,000; M = 0.25.

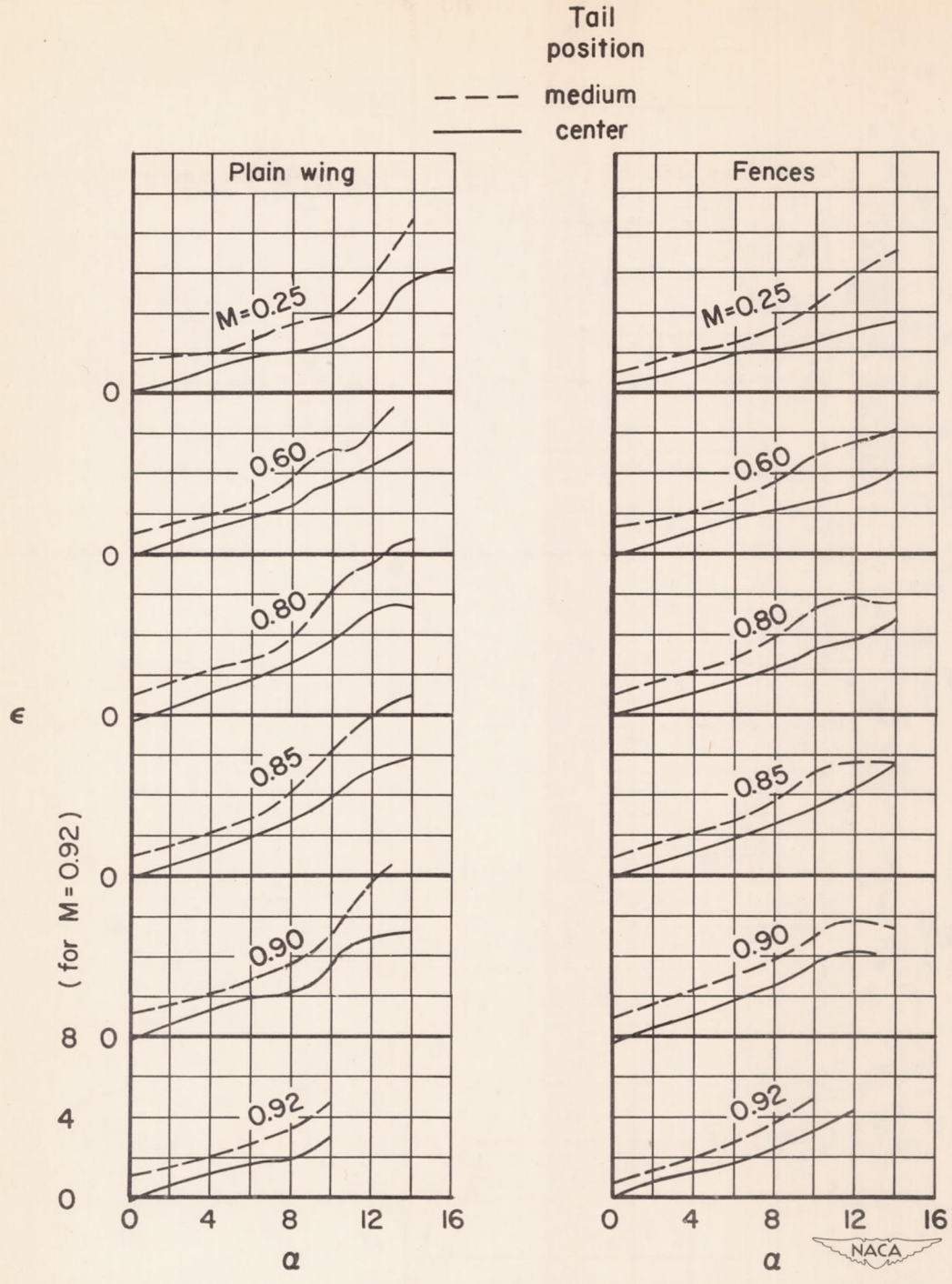

Figure 23.- The variation of effective downwash at the tail with angle of attack for the model with and without fences at various Mach numbers; R = 2,000,000.

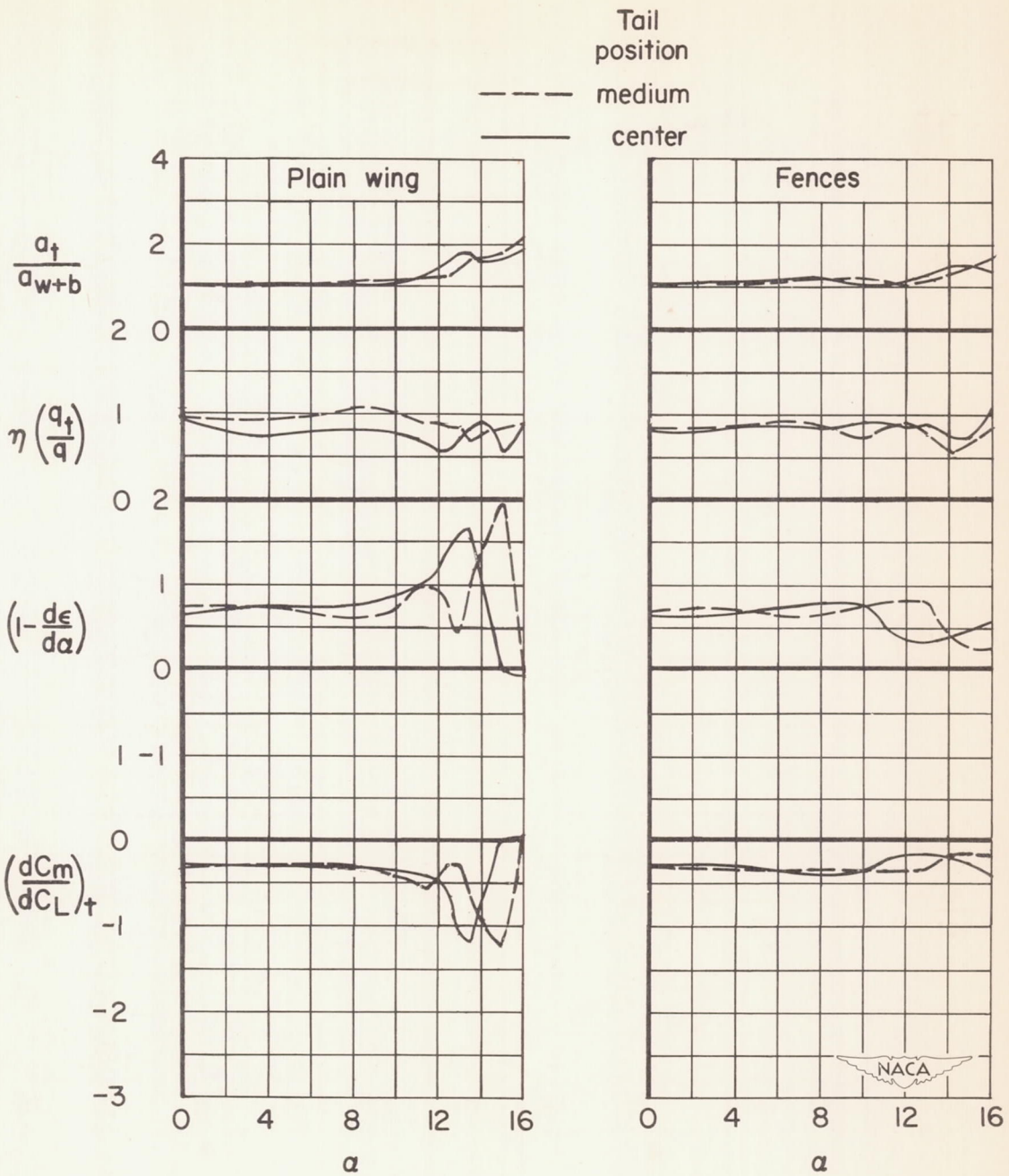

Figure 24.- The variation with angle of attack of the tail stability parameter and the factors affecting the stability contribution of the horizontal tail at a Reynolds number of 10,000,000; M = 0.25.

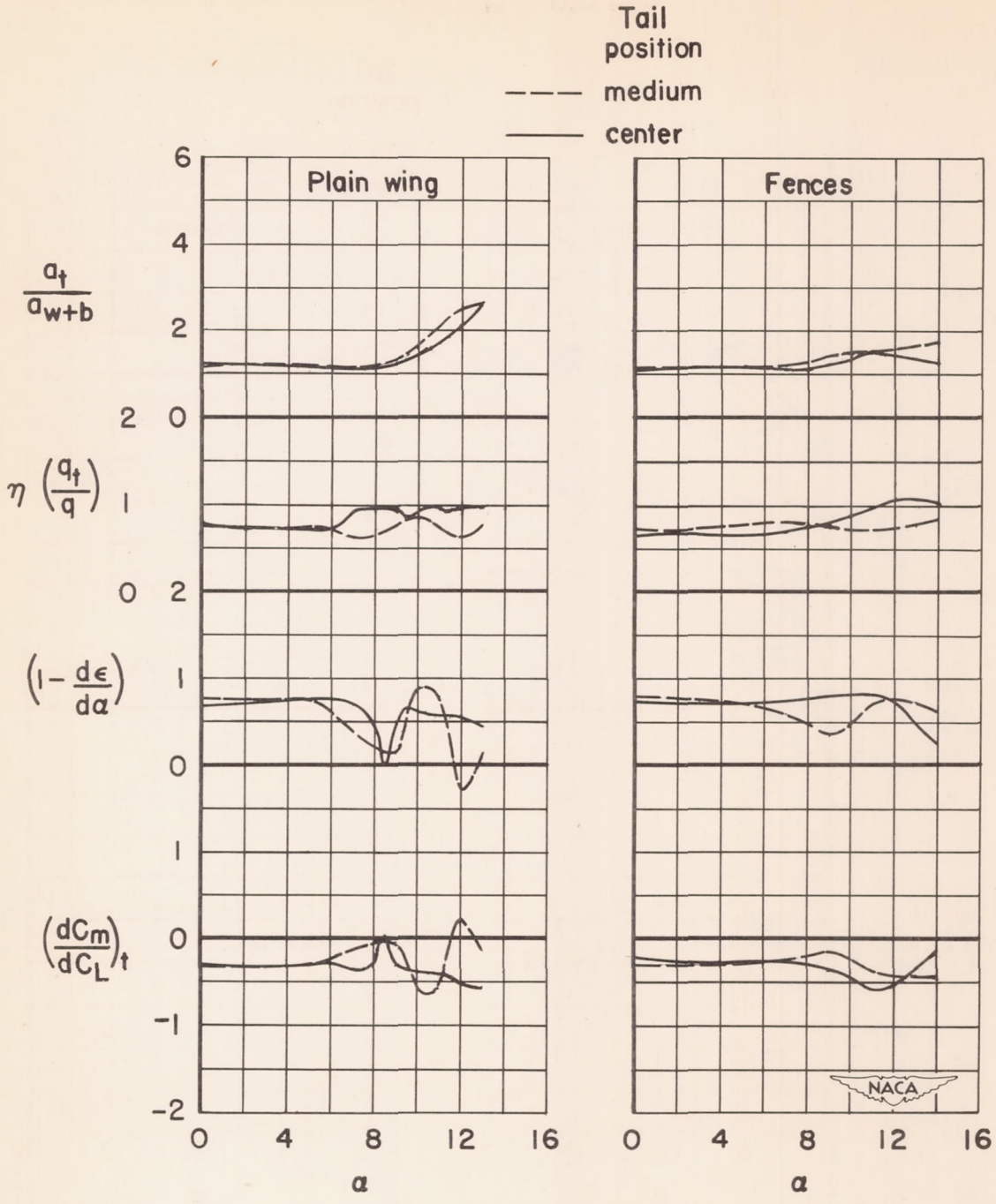

(a) M = 0.60

Figure 25.- The variation with angle of attack of the tail stability parameter and the factors affecting the stability contribution of the horizontal tail; R = 2,000,000.

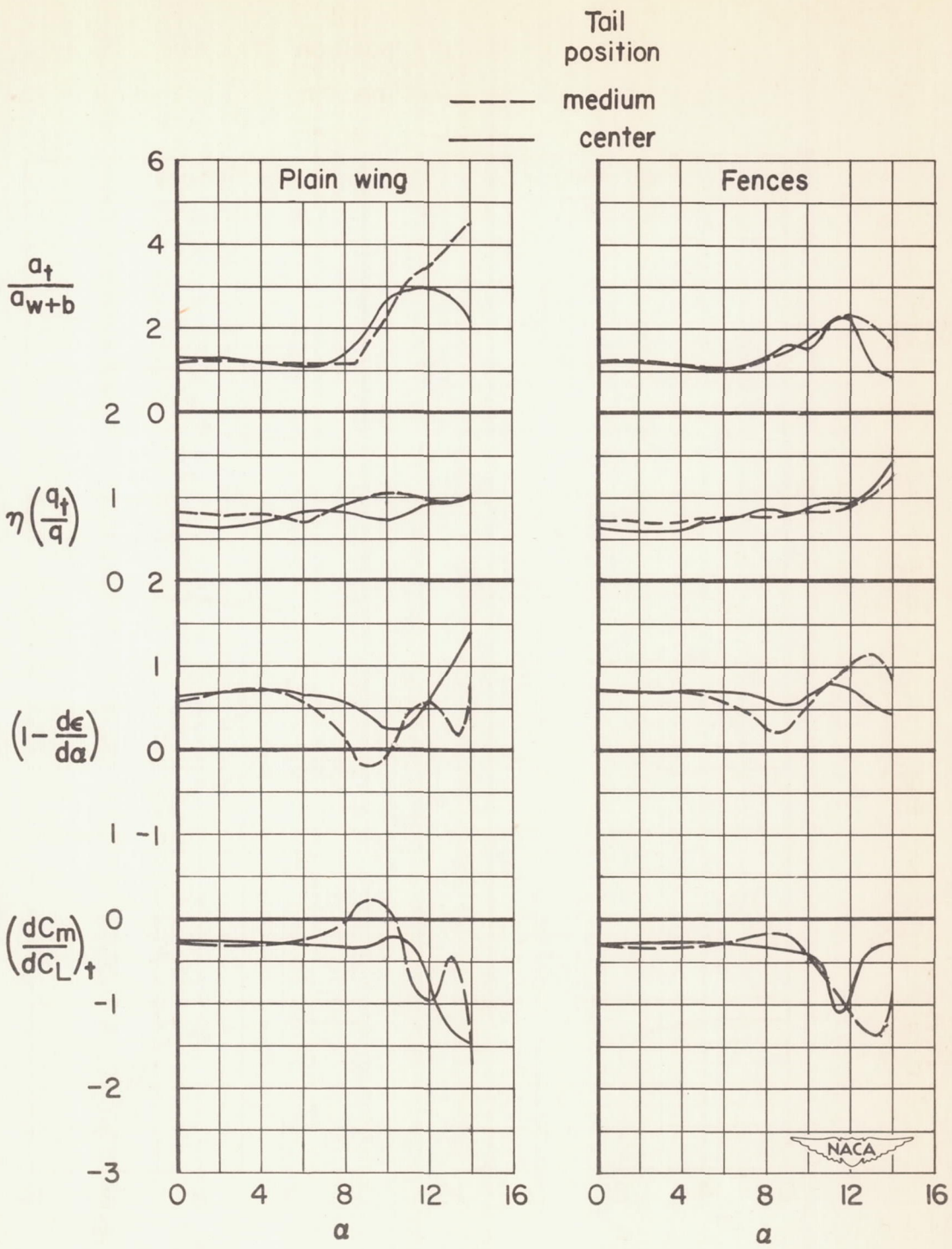

(b) M = 0.80

Figure 25.- Continued.

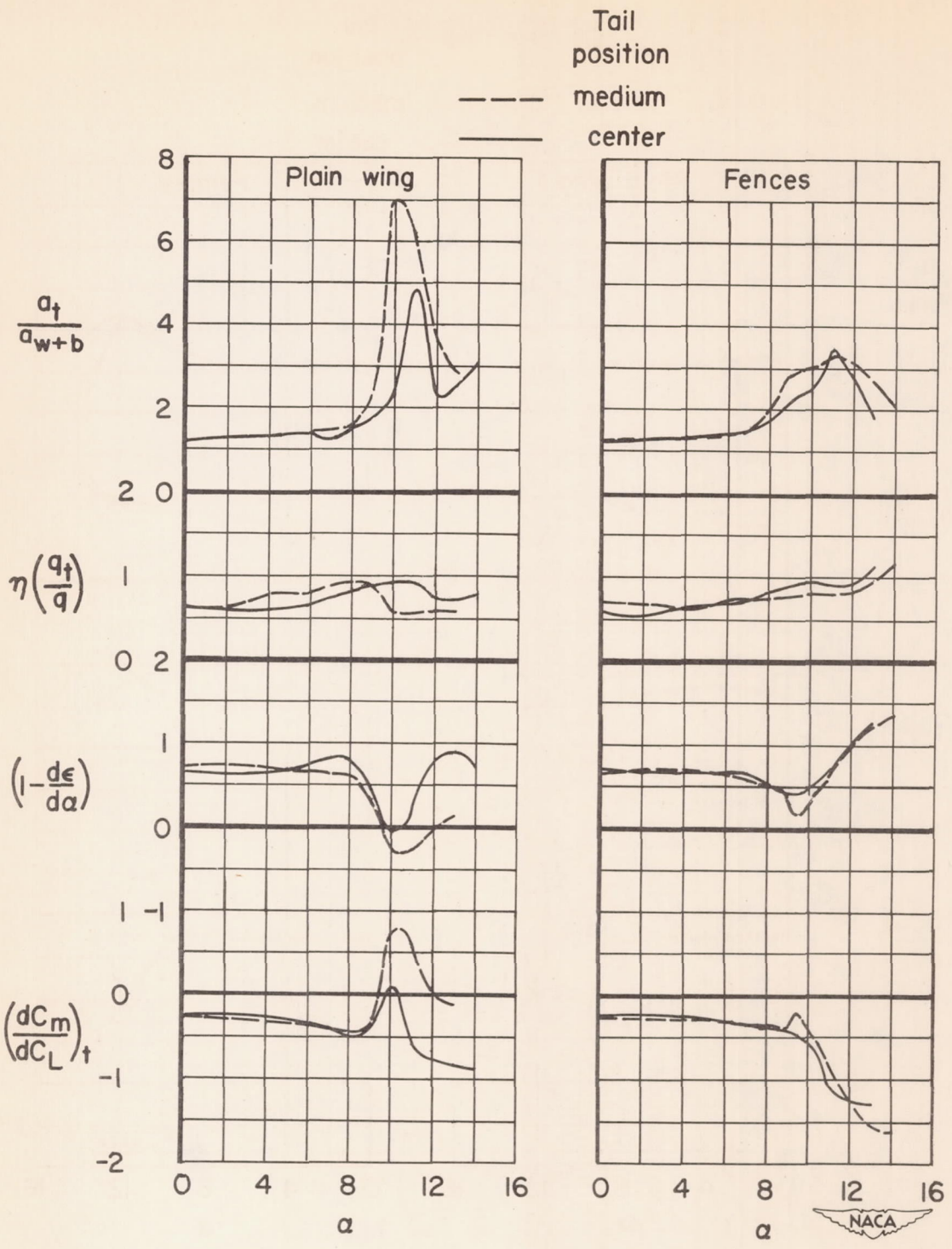

(c) M = 0.90

Figure 25.- Concluded.

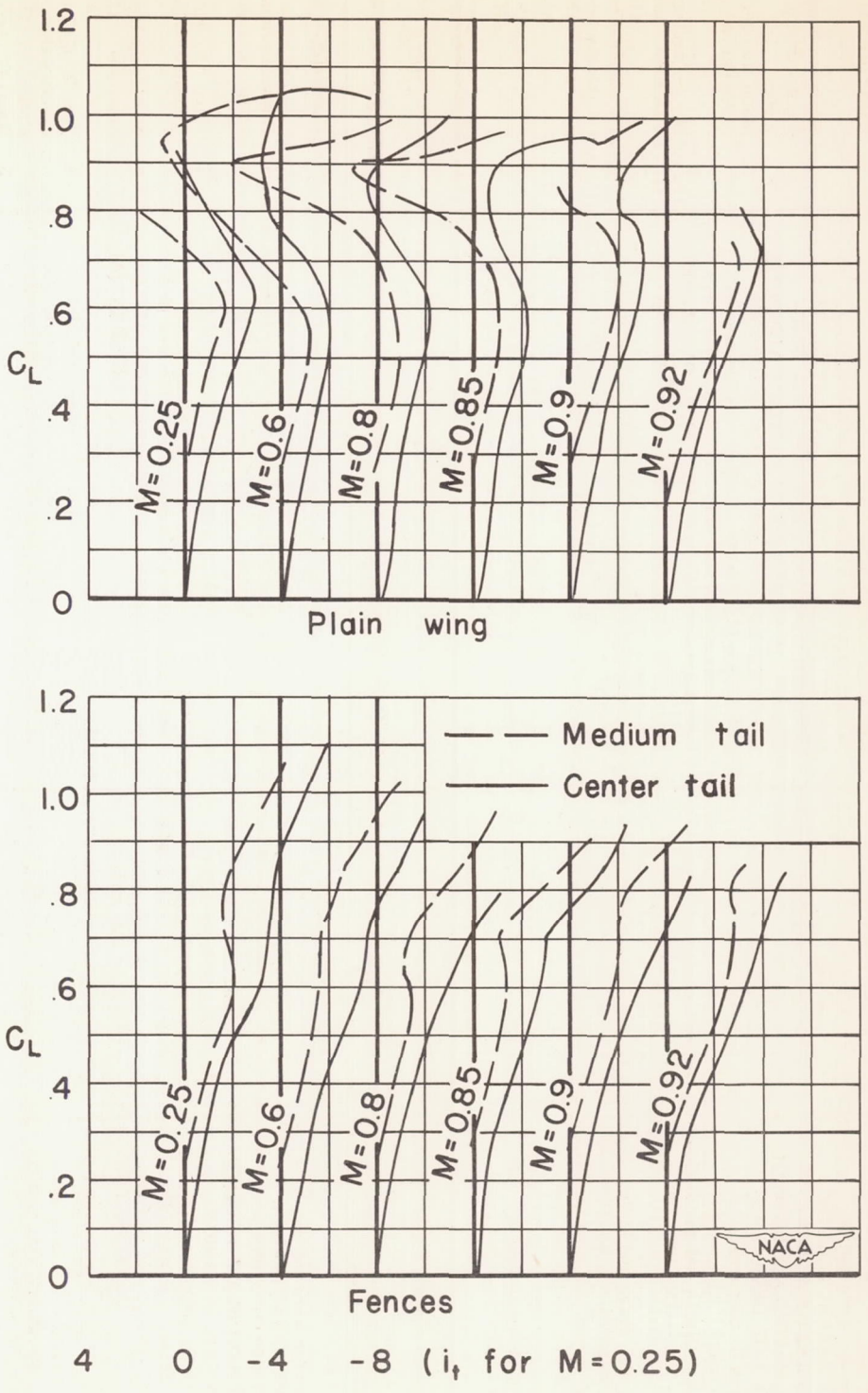

Figure 26.- The variation of tail incidence for longitudinal balance with lift coefficient at various Mach numbers; c.g. at $0.44\bar{c}$, R = 2,000,000.

NACA-Langley - 1-28-55 - 350